Critical Casimir torques and forces
acting on needles in two spatial dimensions

O. A. Vasilyev[1,2], E. Eisenriegler[3], and S. Dietrich[1,2]

[1] Max-Planck-Institut für Intelligente Systeme, Heisenbergstraße 3, D-70569 Stuttgart, Germany
[2] IV. Institut für Theoretische Physik, Universität Stuttgart,
Pfaffenwaldring 57, D-70569 Stuttgart, Germany
[3] Theoretical Soft Matter and Biophysics, Institute of Complex Systems,
Forschungszentrum Jülich, D-52425 Jülich, Germany

(Dated: April 16, 2013)

We investigate the universal orientation-dependent interactions between non-spherical colloidal particles immersed in a critical solvent by studying the instructive paradigm of a needle embedded in bounded two-dimensional Ising models at bulk criticality. For a needle in an Ising strip the interaction on mesoscopic scales depends on the width of the strip and the length, position, and orientation of the needle. By lattice Monte Carlo simulations we evaluate the free energy difference between needle configurations being parallel and perpendicular to the strip. We concentrate on *small* but nonetheless mesoscopic needle lengths for which analytic predictions are available for comparison. All combinations of boundary conditions for the needles and boundaries are considered which belong to either the "normal" or the "ordinary" surface universality class, i.e., which induce local order or disorder, respectively. We also derive exact results for needles of *arbitrary* mesoscopic length, in particular for needles embedded in a half plane and oriented perpendicular to the corresponding boundary as well as for needles embedded at the center line of a symmetric strip with parallel orientation.

I. INTRODUCTION

A solvent near its bulk critical point induces long-ranged forces between immersed mesoscopic particles which are "universal", i.e., independent of most microscopic details of the system [1–4]. Apart from a few bulk properties of the solvent and from its local interactions with the surfaces of the immersed particles, these forces depend only on the *geometry of the confinement* of the critical fluctuations of the solvent imposed by the particle surfaces, that is on the sizes, shapes, positions, and orientations of the particles. Such forces have been observed experimentally in film geometry for ^{4}He [5, 6] and ^{3}He/^{4}He mixtures [7] near the superfluid transition as well as for classical binary liquid mixtures near their demixing transition [8] and, directly, between a single spherical particle immersed in a binary liquid mixture near the critical demixing point and its confining planar wall [9, 10]. Due to the similarity of these forces with the Casimir forces arising in quantum electrodynamics [11, 12] they are called critical Casimir forces.

Nonspherical particles near other confinements, such as a planar wall, experience orientation dependent forces giving rise to critical Casimir *torques* [13, 14].

In the following we concentrate on critical solvents belonging to the Ising universality class such as demixing classical binary liquid mixtures. In these systems the particle surfaces generically prefer one of the two components of the mixture, i.e., in Ising language one of the two directions ($+$ or $-$) of the order parameter is preferred. This preference is captured in terms of surface fields the strength of which under renormalization group flow attains $\pm\infty$, corresponding to fixed surface spins and denoted by $\pm$ boundary conditions. However, using

suitable surface preparation one can suppress this preference, being left with a weakened tendency to demix near the particle surface [15]. These two types of surface universality classes [16] are called "normal" ($+/-$) and "ordinary" (O), respectively.

Simple universal behavior arises in the scaling region where the ranges of the interactions between the ordering degrees of freedom other than short-ranged ones and the lengths characterizing corrections to scaling and the crossover from less stable bulk and surface universality classes, respectively, are much smaller than the increasing correlation length of the bulk solvent upon approaching criticality, than the distances between the particles, and than the lengths characterizing the sizes and shapes of the particles. In this region of a clear separation of "microscopic" and "mesoscopic" lengths, the forces and torques are given by universal scaling functions which, apart from the surface universality classes, only depend on ratios of the characteristic mesoscopic lengths.

Here, our main interest is in the orientation dependent interaction of nonspherical particles with boundaries of critical systems. For the interaction between a prolate uniaxial ellipsoid and a planar wall with $++$ or $+-$ boundary conditions at the corresponding surfaces the complete universal scaling functions for the critical Casimir forces, both for the disordered and ordered bulk phases, have been obtained within mean field theory [14]. Beyond mean field theory such scaling functions have been determined to a lesser degree of completeness. For *nearby* particles, i.e., for closest surface to surface distances much smaller than their size and radii of curvature, the interaction can be expressed in terms of the Casimir force in film geometry by using the Derjaguin approximation. The scaling function of the latter is avail-

able for ++ and +− surfaces in three [17–19] and two [20] spatial dimensions [21]. For a *small* spherical [22] or non-spherical [13, 23] particle, with a size much smaller than the bulk correlation length and the distances to the surfaces of other particles or to boundaries, the interactions can be obtained from the so-called "small particle expansion" [24]. This is one of the field theoretic operator expansions for small objects the most well known of which is the product of two nearby operators first considered around 1970 by Wilson, Polyakov, and Kadanoff [25, 26]. These expansions are to a certain extent reminiscent of the multipole expansion in electrostatics.

In view of the twofold asymptotic condition, i.e., the particle being *small* on mesoscopic scales and *large* on the microscopic scale [24], it is a nontrivial issue under which circumstances the results of the "small particle expansion" can be observed for a given actual system. As a first step to address this issue, here we investigate whether the results of the expansion can be observed in the two-dimensional Ising model on a square lattice with (ferromagnetic) couplings $\mathcal{J} > 0$ between nearest neighbor spins only and right at the bulk critical point.

In our Monte Carlo simulations we consider a lattice of finite size with the form of a strip (or rectangle) comprising W rows and L columns with an embedded particle resembling a needle. The directions along the rows and columns define, respectively, the directions u and v parallel and perpendicular to the strip of length [27] L and width W. While in the u direction we impose periodic boundary conditions by means of couplings $\mathcal{J}$ between the first and last spin in each row, we couple all of the spins in the lowest and uppermost row by means of interactions 0 or $\pm\mathcal{J}$ to spins which are *fixed* in the + direction and are located in outside neighboring rows (see Fig. 1). Thus in the v direction, the strip is bounded by free surfaces or surfaces to which a magnetic field $\propto \pm\mathcal{J}$ is applied, i.e., by surfaces of "ordinary" (O) or "normal" ($+/-$) character.

In order to generate an embedded needle with O or $+/-$ boundary conditions and orientation parallel to the strip we remove couplings (break bonds) between two neighboring lattice rows or we fix spins within a single lattice row, respectively (see Fig. 1). In the two cases we define the length D of the needle as the number [27] of broken bonds and of fixed spins, respectively, which we choose to be even and odd, respectively, in order that the needle centers × coincide with the center of an elementary square and a vertex of the lattice, respectively. This allows us to "turn" the needles abruptly about their center by 90 degrees upon rearranging the broken bonds and fixed spins, leading to broken bonds between neighboring columns and fixed spins within a single column of the lattice, respectively. In order to be able to position the centers of O and $+/-$ needles right at the midline of the strip (as shown in Fig. 1) we choose W to be even and odd, respectively.

In the simulation we calculate the free energy expense ΔF required to "turn" the needle about its center from
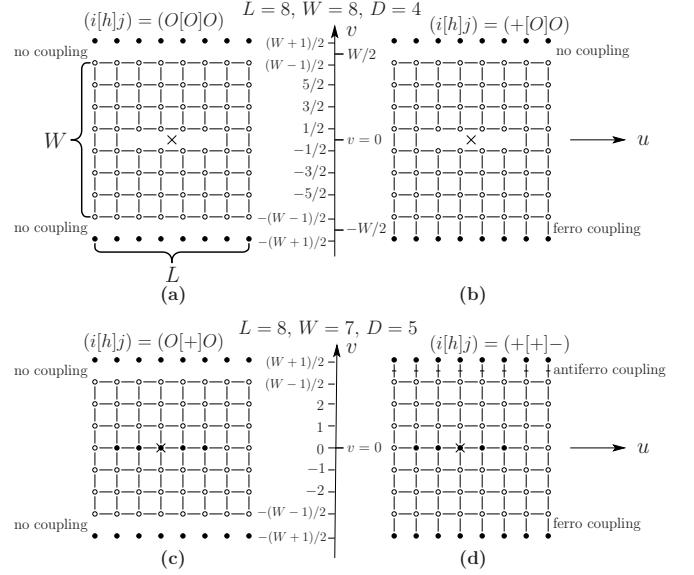
FIG. 1: Needle, with their centers denoted by ×, embedded in a strip of a ferromagnetic Ising model on a square lattice comprising W rows and L columns [27] of fluctuating spins (empty circles) and periodic boundary condition in the u direction parallel to the rows. The two additional rows of spins fixed in the + direction (full circles) allow one to induce positive or negative magnetic fields at the surfaces of the strip by coupling them in a ferro- or antiferromagnetic way to the bottom and top rows of fluctuating spins (see the main text). (a) and (b): Needle of $D = 4$ broken bonds in a strip with the number W of rows and the number L of columns equal to $W = L = 8$. (a) shows the case $(O[O]O)$ of a strip with two free surfaces (no coupling to the fixed spins) while (b) shows the case $(+[O]O)$ in which a ferromagnetic coupling to the fixed spins leads to a positive magnetic field at the lower surface. (c) and (d): Needle of $D = 5$ spins fixed in the + direction (full circles) in a strip with $W = 7$ and $L = 8$. (c) shows the case $(O[+]O)$ while (d) shows the case $(+[+]-)$ with positive and negative magnetic fields induced at the lower and upper surfaces by ferro- and antiferromagnetic couplings, respectively. All the needles shown are oriented in the u direction and have their center × at the midline $v = 0$ of the strip, half way between the strip surfaces, i.e., $v_N = 0$ for the vertical position of the center of the needle. This requires to choose W even (odd) for needles of broken bonds (of fixed spins) so that spins reside at half odd integer (integer) values of v. Needles oriented in the v direction are shown in Figs. 6 and 7 below.

an alignment perpendicular to the strip to the parallel alignment. This is a measure for the effective *torque* acting on the needle. In line with the introductory remarks the free energy cost ΔF depends on the distances of the needle center from the strip surfaces.

We put the origin of the (u, v) coordinate system at the midline of the lattice, i.e., for O and $+/-$ needles at the center of an elementary square and at a vertex so that the lattice spins are located at half odd integer and integer values, respectively, of the coordinates (see Fig. 1). With this choice the mirror symmetry of ΔF in a strip

with equal boundary conditions $i = j$ is described simply by its invariance if the coordinate $v = v_N$ of the needle center changes sign. Here i and j denote the boundary conditions at the surfaces at $v = -W/2$ and $v = W/2$, respectively. Figure 1 shows the special case in which the centers $\times$ of O and $+/-$ needles coincide with the origin, i.e., v_N vanishes, while in the general case v_N takes integer values for both types of needles.

It is useful to adopt a notation $(i[h]j)$ which characterizes the boundary conditions i and j of the strip surfaces as well as the boundary condition h of the embedded needle. For example, $(+[+]-)$ denotes the case of a needle of spins fixed in the $+$ direction which is embedded in a strip with outside couplings $\mathcal{J}$ and $-\mathcal{J}$ at the lower and upper surfaces inducing strip surfaces $i = +$ and $j = -$, respectively, as shown in Fig. 1(d).

For completeness we consider also the case of a strip with periodic boundary conditions in both u and v directions by coupling, in both the W rows and in the L columns, the corresponding end spins to each other with strength $\mathcal{J}$. This is a strip without surfaces and is equivalent to a square lattice on a torus.

If D, W, L, and the closest distance between the needle and the strip boundaries (corresponding to a_N and $a_<$ in Figs. 2(a) and 2(b), respectively) are "sufficiently" large on the scale of the lattice constant, the free energy cost ΔF in the lattice model is expected to display universal scaling behavior and, as mentioned above, $\Delta F/(k_B T)$ will depend only on the universality classes $(i[h]j)$ of the boundaries and the needle and on three independent ratios of D, W, L, and v_N. In this case one

can adopt a mesoscopic continuum description with sharp strip boundaries at $v = \pm W/2$ since lengths only differing by approximately a lattice constant can be identified. Likewise, different microscopic definitions of the length of the needles, such as the number $D - 1$ of bonds between the fixed spins of a $+$ needle (instead of its D fixed spins), lead to the same mesoscopic length D. Figure 2 shows the various lengths characterizing the geometry of a needle in a strip within the continuum description.

For small mesoscopic needles and a long strip, i.e., for $D \ll W \ll L$, the universal behavior can be predicted by means of the "small particle expansion" and, as mentioned earlier, it is one of our main goals to quantitatively investigate whether present Monte Carlo simulations can access this regime.

For a needle perpendicular to the boundary of a half plane or embedded at the midline of a symmetric $(i = j)$ strip of infinite length, we derive the analytic form of the universal scaling behavior of the critical Casimir forces in the *complete* range of mesoscopic needle lengths D, increasing from small to large. This aspect is interesting in its own right and also allows us to estimate the range of validity of the "small needle expansion".

The predictions of the "small particle expansion" for ΔF in critical Ising strips and our analytic results for needles of arbitrary length are presented in Secs. II and III, respectively. In Sec. IV we describe the lattice model in more detail and explain how one obtains via Monte Carlo simulations the results for ΔF which are compared with the analytic scaling predictions in Sec. V . Our results are summarized in Sec. VI. In Appendices A and B we present the input material and the derivations which are necessary in order to obtain the predictions and results of Secs. II and III, respectively. For the convenience of the reader we present a glossary of our symbols and notations in Appendix C.

Besides for critical systems [13, 14] the orientation dependent interaction between a wall and a nonspherical mesoscopic object (such as an ellipsoid, a semi-infinite plate, or a spherocylinder) has been studied also for quantum electrodynamics [28, 29] and for purely entropic systems in which it is induced by spherical so-called depletion agents with hard body interaction only [30] or by free nonadsorbing polymer chains [23]. As for correlation-induced forces we mention also the attractive effective force generated by needles (rigid rods) acting as depletion agents [31] and the repulsive force generated by a nonadsorbing polymer chain grafted to the tip of a (model-) atomic force microscope near a repulsive wall [32]. Finally we note that the critical Casimir force between inclusions in the *two*-dimensional Ising model has been suggested as a possible mechanism for the presence of long-ranged forces between membrane bound proteins [33], which are typically non-circular.


FIG. 2: Continuum [27] description of the geometry of a needle in a strip. In the strip of length L and width W the embedded needle of length D is oriented parallel (a) and perpendicular (b) to the strip boundaries at $v = \pm W/2$. The needle center $\times$ is located at $u = u_N = 0$ and $v = v_N < 0$ at a distance $a_N \equiv v_N + W/2 > 0$ from the lower boundary. In the perpendicular orientation the closer end of the needle has a distance $a_< \equiv a_N - D/2 > 0$ (and the farther end a distance $a_> = a_< + D$) from the lower boundary.

II. SMALL NEEDLE EXPANSION

Here we specialize the "small particle expansion" for non-spherical particles (see Ref. [13]) to the present case of a needle embedded in the two-dimensional Ising model and apply it to the geometry of a needle in a strip.

We consider a needle of small mesoscopic length D, centered at $\mathbf{r}_N$, and pointing along the unit vector $\mathbf{n}$. Inserting the needle into the $d = 2$ Ising model at its critical point [34] changes the Boltzmann weight of the corresponding field theory by a factor $\exp(-\delta\mathcal{H})$ which can be represented by the operator [26] expansion [13, 23]

$$\exp(-\delta\mathcal{H}) \propto 1 + S_I + S_A \qquad (2.1)$$

where

$$S_I = \sum_{\mathcal{O}=\phi,\epsilon} \mathcal{A}_{\mathcal{O}}^{(h)} \left[\left(\frac{D}{2}\right)^{x_{\mathcal{O}}} + \right.$$
$$\left. + \frac{1}{16x_{\mathcal{O}}} \left(\frac{D}{2}\right)^{2+x_{\mathcal{O}}} \Delta_{\mathbf{r}_N} \right] \mathcal{O}(\mathbf{r}_N) + ... \qquad (2.2)$$

with $\Delta_{\mathbf{r}_N} = \nabla_{\mathbf{r}_N}^2$ and

$$S_A = \sum_{k,l=1,2} \left(n_k n_l - \frac{\delta_{kl}}{2} \right) \left[-\frac{\pi}{2} \left(\frac{D}{2}\right)^2 T_{kl}(\mathbf{r}_N) + \right.$$
$$\left. + \sum_{\mathcal{O}=\phi,\epsilon} \mathcal{A}_{\mathcal{O}}^{(h)} \frac{3}{8(1+x_{\mathcal{O}})} \left(\frac{D}{2}\right)^{2+x_{\mathcal{O}}} \partial_{(r_N)_k} \partial_{(r_N)_l} \mathcal{O}(\mathbf{r}_N) \right]$$
$$+ ... \qquad (2.3)$$

are the isotropic and anisotropic contributions, respectively. Here $\mathcal{O} = \phi$ is the order-parameter-density operator and $\mathcal{O} = \epsilon$ is the difference of the energy-density [35] operator e and its average $\langle e \rangle_{\text{bulk}}$ in the unbounded plane (bulk) at bulk criticality (so that their bulk averages $\langle\phi\rangle_{\text{bulk}}$ and $\langle\epsilon\rangle_{\text{bulk}}$ vanish at the bulk critical point). They are normalized such that the bulk two-point correlation functions [34] are [36]

$$\langle \mathcal{O}(\mathbf{r})\mathcal{O}(\mathbf{r}') \rangle_{\text{bulk}} = |\mathbf{r} - \mathbf{r}'|^{-2x_{\mathcal{O}}}, \qquad (2.4)$$

where (in $d = 2$) $x_\phi = 1/8$ and $x_\epsilon = 1$ are their scaling dimensions [37]. The affiliation of the surface of the needle to the "ordinary" ($h = O$) or to the "normal" ($h = +$ or $h = -$) surface universality class enters into Eqs. (2.1)-(2.3) via the universal half plane amplitude $\mathcal{A}_{\mathcal{O}}^{(h)}$. The latter is the amplitude of the profile [34] of $\mathcal{O}$ in the half plane, $\langle\mathcal{O}\rangle_{\text{half plane}} = \mathcal{A}_{\mathcal{O}}^{(h)} a^{-x_{\mathcal{O}}}$, as function of the mesoscopic distance a from the boundary line of type h and is given by [37]

$$\mathcal{A}_\phi^{(O)} = 0, \ \mathcal{A}_\phi^{(+)} = -\mathcal{A}_\phi^{(-)} = 2^{1/8},$$
$$\mathcal{A}_\epsilon^{(O)} = -\mathcal{A}_\epsilon^{(+)} = -\mathcal{A}_\epsilon^{(-)} = 1/2. \qquad (2.5)$$

The properties $\mathcal{A}_\phi^{(O)} = 0$ and $\mathcal{A}_\phi^{(-)} = -\mathcal{A}_\phi^{(+)}$ of the amplitudes of the order parameter profile are obvious from the up-down symmetry of the Ising spins [34]. The energy density profile increases (decreases) upon approaching an "ordinary" ("normal") boundary where the Ising spins are more disordered (more ordered) than in the bulk [35]. This implies the positive (negative) sign of the corresponding amplitude $\mathcal{A}_\epsilon^{(O)}$ ($\mathcal{A}_\epsilon^{(+)} = \mathcal{A}_\epsilon^{(-)}$). The absolute values of $\mathcal{A}_\epsilon^{(O)}$ and $\mathcal{A}_\epsilon^{(+)} = \mathcal{A}_\epsilon^{(-)}$ are the same, due to duality properties [38, 39]. In Eq. (2.3) the contribution from the stress [37] tensor T_{kl} is the same [40] for all needle types $h = O, +, -$.

The ellipses in Eqs. (2.2) and (2.3) stand for contributions of fourth order and higher [41] in the small mesoscopic length D. The common factor of proportionality on the rhs of Eq. (2.1) is given [34] by $\langle\exp(-\delta\mathcal{H})\rangle_{\text{bulk}}$ because the bulk averages of S_I and S_A vanish at the bulk critical point.

For a two-dimensional Ising model with boundaries the insertion free energy of the needle depends on its position and orientation with respect to these boundaries. Removing the needle from the bulk model and inserting it in the bounded one at a distance from the boundaries much larger than D changes the free energy by $F(\mathbf{r}_N, \mathbf{n}) = -k_B T \ln\langle(1+S_I+S_A)\rangle_{\text{BM}}$ where BM denotes the bounded model in the absence of the needle. We shall concentrate on the geometry of a needle in a strip as described in the Introduction (see Fig. 2) for which BM $\equiv$ ST is the strip with boundaries (i, j) in the absence of the needle and correspondingly use the notation [27]

$$\mathbf{r}_N = (u_N, v_N), \quad \mathbf{n} = (n_{||}, n_\perp) \qquad (2.6)$$

for the center and direction vectors of the needle with the components parallel and perpendicular to the strip. The density averages $\langle\mathcal{O}\rangle_{\text{ST}}$ at $\mathbf{r}_N$ which enter $\langle S_I + S_A \rangle_{\text{ST}}$ are, within this model, independent of u_N and in the scaling region given by

$$\langle\mathcal{O}(\mathbf{r}_N)\rangle_{\text{ST}} = W^{-x_{\mathcal{O}}} f_{\mathcal{O}}^{(i,j)}(v_N/W, W/L), \qquad (2.7)$$

where f are universal scaling functions and $f_{\mathcal{O}}^{(j,i)}$ follows from $f_{\mathcal{O}}^{(i,j)}$ upon replacing v_N/W by $-v_N/W$.

Due to the continuity equation of the stress tensor [37] its average $\langle T_{kl}(\mathbf{r}_N)\rangle_{\text{ST}}^{(i,j)}$ in the strip is independent of both u_N and v_N and follows from the universal, scale-free, and shape-dependent contribution [42] $\Phi_{\text{ST}}^{(i,j)}(L/W)$ to the free energy F_{ST} per $k_B T$ of the strip ST without the needle:

$$\langle[T_{\perp\perp}, T_{||||}]\rangle_{\text{ST}}^{(i,j)} = -[L^{-1}\partial_W, W^{-1}\partial_L]\Phi_{\text{ST}}^{(i,j)}(L/W)$$
$$= [1, -1]W^{-2}\Delta_{i,j}(W/L). \qquad (2.8)$$

Like in Eq. (2.6), here $||$ and $\perp$ denote directions parallel and perpendicular to the u axis of the strip,

$$\Delta_{i,j}(W/L) = (d/d\delta)\Phi_{\text{ST}}^{(i,j)}(\delta), \quad \delta = L/W, \qquad (2.9)$$

and the off-diagonal components $\langle T_{\perp\parallel}\rangle_{\mathrm{ST}} = \langle T_{\parallel\perp}\rangle_{\mathrm{ST}}$ vanish by symmetry. Cardy [43] has obtained an explicit form for all functions $\Phi_{\mathrm{ST}}^{(i,j)}(\delta)$. While an extensive discussion of $\Delta_{i,j}(W/L)$ is deferred to Appendix A 2, here we mention a few basic properties. Obviously $\Phi_{\mathrm{ST}}^{(i,j)}$ and $\Delta_{i,j}$ are symmetric in i and j. For a long strip the leading behavior $\Phi_{\mathrm{ST}}^{(i,j)}(L/W \to \infty) = \Delta_{i,j}(0) \times \delta$ of $\Phi_{\mathrm{ST}}^{(i,j)}$ is linear in δ with $\Delta_{i,j}(0) \equiv \Delta_{i,j}$ given [37] by $\Delta_{i,j} = (\pi/48)[-1, -1, 23, 2]$ for $(i,j) = [(O,O), (+,+), (+,-), (+,O)]$. While due to the $(+ \leftrightarrow -)$ symmetry the equalities $\Delta_{+,+}(1/\delta) = \Delta_{-,-}(1/\delta)$ and $\Delta_{+,O}(1/\delta) = \Delta_{-,O}(1/\delta)$ hold for arbitrary $1/\delta$, the equality $\Delta_{O,O} = \Delta_{+,+}$ holds only for infinitely long strips [44], i.e., $1/\delta = 0$.

For the free energies $F_\parallel$ and $F_\perp$ associated with removing the needle from the bulk system and inserting it in the strip with its center at $\mathbf{r}_N$ and with its orientation $\mathbf{n}$ parallel and perpendicular, respectively, to the u axis, Eqs. (2.1)-(2.3) and (2.6) yield

$$F_\parallel \equiv F(\mathbf{r}_N, \mathbf{n} = (1,0)) = -k_B T \ln Z_\parallel \qquad (2.10)$$

and

$$F_\perp \equiv F(\mathbf{r}_N, \mathbf{n} = (0,1)) = -k_B T \ln Z_\perp \qquad (2.11)$$

with

$$Z_\parallel = 1 + \zeta_I - \zeta_A, \quad Z_\perp = 1 + \zeta_I + \zeta_A \qquad (2.12)$$

where

$$\zeta_I = \sum_{\mathcal{O}=\phi,\epsilon} \mathcal{A}_{\mathcal{O}}^{(h)} \left[\left(\frac{D}{2W}\right)^{x_{\mathcal{O}}} + \frac{1}{16 x_{\mathcal{O}}} \left(\frac{D}{2W}\right)^{2+x_{\mathcal{O}}} \times \right.$$
$$\left. \times \frac{\partial^2}{\partial (v_N/W)^2} \right] f_{\mathcal{O}}^{(i,j)} \left(\frac{v_N}{W}, \frac{W}{L}\right) + \dots \quad (2.13)$$

and

$$\zeta_A = -\frac{\pi}{2} \left(\frac{D}{2W}\right)^2 \Delta_{i,j}\left(\frac{W}{L}\right) + \frac{1}{2} \sum_{\mathcal{O}=\phi,\epsilon} \frac{3\mathcal{A}_{\mathcal{O}}^{(h)}}{8(1+x_{\mathcal{O}})} \times$$
$$\times \left(\frac{D}{2W}\right)^{2+x_{\mathcal{O}}} \frac{\partial^2}{\partial (v_N/W)^2} f_{\mathcal{O}}^{(i,j)} \left(\frac{v_N}{W}, \frac{W}{L}\right) + \dots (2.14)$$

follow from S_I and S_A in Eqs. (2.2) and (2.3), respectively. This implies the expression

$$\Delta F = -k_B T \ln(Z_\parallel / Z_\perp) \qquad (2.15)$$

for the free energy required to turn the needle about its center from its orientation perpendicular to the u axis of the strip to the parallel orientation.

In the expansions in Eqs. (2.13) and (2.14) a term $\propto D^{\mathcal{X}}$ is of the order of $(D/W)^{\mathcal{X}}$ near the strip center, where $|v_N| \ll W$, and of the order of $(D/a_N)^{\mathcal{X}}$ near the strip boundaries, where $a_N \equiv (W/2) - |v_N| \ll W$.

These expansions for the *partition functions* $Z_\parallel$ and $Z_\perp$ are useful if D/W and D/a_N are much smaller than 1. However, expanding the *free energies* $F_\parallel$, $F_\perp$, and ΔF in powers of D is not always useful for the comparison with our simulation data. While $D/W \ll 1$ and $D/a_N \ll 1$ can readily be achieved in the MC simulations for a needle with a mesoscopic length D of many lattice constants, at present it seems to be unrealistic to achieve $(D/W)^{1/8} \ll 1$ and $(D/a_N)^{1/8} \ll 1$. Thus we expand the logarithm in Eq. (2.15) in terms of powers of D only in those cases in which the power $D^{x_\phi} \equiv D^{1/8}$ does not appear [45] in Eq. (2.13). These are the cases with an "ordinary" needle $h = O$, for which $\mathcal{A}_\phi^{(h)}$ vanishes, and with a "normal" needle in a strip with two "ordinary" boundaries $i = j = O$, for which the density profile in Eq. (2.7) vanishes for the order parameter $\mathcal{O} = \phi$. Expanding the logarithm in these cases yields

$$\Delta F = \Delta F_l + \Delta F_{nl} + \dots \qquad (2.16)$$

with the leading contribution

$$\frac{\Delta F_l}{k_B T} = -\pi \left(\frac{D}{2W}\right)^2 \Delta_{i,j}(W/L) \qquad (2.17)$$

and the next-to-leading contribution

$$\frac{\Delta F_{nl}}{k_B T} = \left(\frac{D}{2W}\right)^3 \mathcal{A}_\epsilon^{(h)} \left[\pi \Delta_{i,j}(W/L) + \right.$$
$$\left. + \frac{3}{16} \frac{\partial^2}{\partial (v_N/W)^2} \right] f_\epsilon^{(i,j)} \left(\frac{v_N}{W}, \frac{W}{L}\right) . (2.18)$$

The ellipses in Eq. (2.16) are of order D^4.

For completeness we also consider a double periodic rectangle or strip with periodic boundary conditions in both the u and v-directions, i.e., the surface of a torus. In this boundary-free case at T_c the average of ϕ vanishes in the strip, that of ϵ is independent of both u and v, and for the average of the stress tensor Eq. (2.8) again applies with $\Delta_{i,j}(W/L)$ replaced by a function $\Delta_P(W/L) = (d/d\delta)\Phi_{\mathrm{ST}}^{(P)}(\delta)$ with the infinite strip limit $\Delta_P(0) \equiv \Delta_P = -\pi/12$ (see Subsec. V A and Appendix A 1 for more details). For the double periodic strip Eqs. (2.16)-(2.18) also apply if $\Delta_{i,j}(W/L)$ and $f_\epsilon^{(i,j)}(v_N/W, W/L)$ are replaced by the corresponding stress amplitude $\Delta_P(W/L)$ and the energy density scaling function $f_\epsilon^{(P)}(W/L)$ which is independent of v_N/W.

Explicit expressions for the functions $\Delta(W/L)$ are known [43] for all types of strips considered here. Concerning the scaling functions $f_{\mathcal{O}}$ the dependence on the aspect ratio W/L is known [46, 47] for $f_\epsilon^{(P)}$ while in the presence of boundaries the functions $f_{\mathcal{O}}^{(i,j)}(v_N/W, W/L)$ are, to the best of our knowledge, known only [48] for $W/L = 0$, i.e., for strips of infinite [49] length $L = \infty$. For the convenience of the reader we collect these expressions in Appendix A.

For the special case in which the distance $a_N = v_N + W/2$ of the center of the small needle of type h from the boundary of type i at $v = -W/2$ (see Fig. 2) is much smaller than the width of the infinitely long strip, i.e., for the case $D \ll a_N$ and W/a_N, $L/a_N \to \infty$, the above expressions for the needle in the strip with free energies $F \equiv F^{(i[h]j)}$ reduce to those for the needle in the *half plane* $v + W/2 \equiv a > 0$ with free energies $F \equiv F^{(i[h])}$ where Eqs. (2.13) and (2.14) are replaced by

$$\zeta_I = \sum_{\mathcal{O}=\phi,\epsilon} \mathcal{A}_{\mathcal{O}}^{(h)} \mathcal{A}_{\mathcal{O}}^{(i)} \left[\vartheta^{x_{\mathcal{O}}} + \frac{1+x_{\mathcal{O}}}{16} \vartheta^{2+x_{\mathcal{O}}} \right] + \dots,$$

$$\zeta_A = \sum_{\mathcal{O}=\phi,\epsilon} \mathcal{A}_{\mathcal{O}}^{(h)} \mathcal{A}_{\mathcal{O}}^{(i)} \frac{3x_{\mathcal{O}}}{16} \vartheta^{2+x_{\mathcal{O}}} + \dots, \qquad (2.19)$$

and Eqs. (2.17) and (2.18) by

$$\frac{\Delta F_l}{k_B T} = 0, \quad \frac{\Delta F_{nl}}{k_B T} = \mathcal{A}_{\epsilon}^{(h)} \mathcal{A}_{\epsilon}^{(i)} \frac{3}{8} \vartheta^3 \qquad (2.20)$$

where

$$\vartheta = \frac{D}{2a_N}. \qquad (2.21)$$

As mentioned above these relations only apply if $0 \le \vartheta \ll 1$.

III. NEEDLES OF ARBITRARY LENGTH

The "small needle expansion" is valid if the mesoscopic length D of the needle is "small" compared to the other mesoscopic lengths of the system, i.e., within the present model much smaller than the width and length of the strip and the distance of the needle from the two boundaries. Given the limited set of operators appearing in Eqs. (2.2) and (2.3), it is an open issue what in this context "small" means quantitatively. In order to get a clue, in this section we study a few situations in which results for an *arbitrary* mesoscopic needle length D can be obtained. These results, which we derive in Appendix B, are interesting also in their own right.

(i) *Needle in half-plane*

We consider a needle of universality class h embedded in the half plane, oriented *perpendicular* to the boundary line of surface universality class i, and with its center located at a distance a_N from the boundary. Here we also introduce the distance $a_< = a_N - (D/2)$ of the closer end of the needle from the boundary (compare Fig. 2(b)) so that one has

$$\vartheta \equiv \frac{D}{2a_N} = \frac{1}{1 + (2a_</D)} \qquad (3.1)$$

for the length ratio ϑ defined in Eq. (2.21). Note that ϑ tends to 0 and 1 for a small (or distant) needle with $D \ll a_N$ and a long (or close) needle with $a_< \ll D$, respectively. Both D and $a_<$ are assumed to

be mesoscopic lengths, i.e., both are large on the microscopic scale. We are interested in the free energy $F_\perp \equiv F_\perp^{(i[h])} = k_B T f_{i[h]}^\perp(\vartheta)$ required to insert the needle from the bulk into the half plane, and in the corresponding Casimir force $-(\partial/\partial a_N)F_\perp^{(i[h])} \equiv -(\partial/\partial a_<)F_\perp^{(i[h])} = (k_B T/a_N)g_{i[h]}^\perp(\vartheta)$ with [50] universal scaling functions $f_{i[h]}$ and $g_{i[h]}$. The above partial derivatives are taken at fixed needle length D. The force pushes the needle away from (towards) the boundary if $g_{i[h]}$ is positive (negative).

Due to symmetries the identities $F_\perp^{(+[+])} = F_\perp^{(-[-])}$, $F_\perp^{(+[O])} = F_\perp^{(-[O])}$, and $F_\perp^{(h[i])} = F_\perp^{(i[h])}$ hold so that exchanging the surface universality classes of the needle and of the boundary leaves the free energy unchanged. These follow from the $(+ \leftrightarrow -)$ and the duality [51] symmetries of the Ising model and are consistent with the symmetries of the corresponding small needle expression which follows from Eqs. (2.11), (2.12), and (2.19).

(ia) For $i = h = O$ the effective interaction has the form (see the paragraph containing Eqs. (B2)-(B4))

$$\frac{F_\perp^{(O[O])}}{k_B T} = f_{O[O]}^\perp(\vartheta) = -2^{-5} \ln \frac{(1+\vartheta)^5}{(1-\vartheta)^3} \qquad (3.2)$$

and is attractive within the entire range $0 \le \vartheta \le 1$. For $\vartheta \ll 1$, Eq. (3.2) is in agreement with the corresponding result $F_\perp^{(O[O])}/(k_B T) = -\vartheta/4 + \vartheta^2/2^5 - \vartheta^3/12 + \mathcal{O}(\vartheta^4)$ of the small needle expansion which follows from Eqs. (2.11), (2.12), and (2.19). For $\vartheta \nearrow 1$, $F_\perp^{(O[O])}/k_B T \to -2^{-5} \times 3 \ln[(2^{2/3}D)/a_<]$ shows a logarithmic dependence. The logarithmic divergence of the free energy for $D/a_< \to \infty$ is related to the long-ranged behavior $\propto 1/a_<$ of the Casimir force for a needle of *infinite* length $D = \infty$ which is addressed in Eq. (3.9) below; its integral diverges for $a_< \to \infty$ (while for a needle of *finite* length D, the force decays more rapidly than $1/a_<$ as $a_<$ increases beyond D so that the integral is finite).

(ib) For $i = +$, $h = O$ the interaction is always repulsive and has the form

$$\frac{F_\perp^{(+[O])}}{k_B T} = 2^{-5} \ln \frac{(1+\vartheta)^3}{(1-\vartheta)^5}, \qquad (3.3)$$

i.e., the same form as Eq. (3.2) but with ϑ replaced by $-\vartheta$ (see Appendix B 1).

(ic) For the Casimir forces, in Appendix B 2 we find expressions which apply to *arbitrary* combinations (i, h) of the universality classes. For later convenience we present them here in two forms

$$-\frac{\partial}{\partial a_N} \frac{F_\perp^{(i[h])}}{k_B T}$$

$$= -\frac{\partial}{\partial a_N} \frac{F_\perp^{(O[O])}}{k_B T} - \frac{1}{2a_N} \frac{1}{1-\vartheta^2} \tilde{\tau}_{i,h}(\vartheta)$$

$$\equiv -\frac{1}{2a_N} \frac{1}{1-\vartheta^2} \left(\frac{1}{12} - \frac{\vartheta^2}{24} - \rho_{i,h}(\vartheta) \right) \qquad (3.4)$$

which are equivalent due to Eq. (3.2) and the definition

$$\tilde{\tau}_{i,h}(\vartheta) \equiv \frac{1}{12}(1 - 6\vartheta + \vartheta^2) - \rho_{i,h}(\vartheta). \quad (3.5)$$

The dependence of $\rho_{i,h}$ on ϑ is given by

$$\rho_{i,h}(\vartheta) = \frac{4\pi\Delta_{i,h}(1/\delta)}{[K^*(\vartheta)]^2} = \frac{\pi\delta^2\Delta_{i,h}(1/\delta)}{4\,[K(\vartheta)]^2} \quad (3.6)$$

with the variable $1/\delta$ replaced by the function

$$1/\delta = K^*(\vartheta)/[4K(\vartheta)] \quad (3.7)$$

of ϑ. Here

$$K^*(\vartheta) \equiv K(\bar{\vartheta}), \quad \bar{\vartheta} \equiv \sqrt{1 - \vartheta^2}, \quad (3.8)$$

and K is the complete elliptic integral function (see Eqs. (8.113.1) and (8.113.3) in Ref. [52]). The quantity $\Delta_{i,h}(1/\delta)$ in Eq. (3.6) is the well-studied [43] Casimir (or stress tensor) amplitude for a strip ST without needle, with boundaries (i, h), and finite aspect ratio $W/L = 1/\delta$ which has been introduced in Eqs. (2.8) and (2.9) and is given explicitly in Appendix A 2.

The symmetries of $F_\perp^{(i[h])}$ addressed above Eq. (3.2) are reflected in Eqs. (3.4)-(3.8) by the symmetries of $\Delta_{i,j}(1/\delta)$ discussed below Eq. (2.9).

For the special cases $(i, h) = (O, O)$ and $(+, O)$ we have checked that Eqs. (3.4)-(3.8) are consistent with the simple expressions given in Eqs. (3.2) and (3.3). In particular, $\tilde{\tau}_{O,O}(\vartheta)$ vanishes for all ϑ.

The present results for a needle embedded in a half plane involve, via $\Delta_{i,h}(1/\delta)$, knowledge about the strip ST without needle but with finite aspect ratio because the two geometries are related by a conformal mapping as explained in Appendix B 2.

Varying ϑ from 0 to 1, for all combinations (i, h) Eqs. (3.4)-(3.8) provide the complete crossover of the force $-(\partial/\partial a_N)F_\perp^{(i[h])}/k_BT$ as the length D and the position (determined by the distances a_N or $a_<$) of the needle in the half plane change from small and remote from the boundary to large and close to the boundary. Equation (3.7) tells us that the corresponding change in the geometry of the strip ST is from remote ($\delta \searrow 0$) to close ($\delta \nearrow \infty$) strip boundaries, as expected.

In the small needle limit $\vartheta \searrow 0$ the quantity $\tilde{\tau}_{i,h}$ vanishes (compare Eq. (A13)) and the expansion for small ϑ is provided by Eqs. (A8), (A10), and (A12) and the form of σ in Eq. (B22). We check in the paragraph containing Eq. (B26) that this expansion is consistent with the small needle expansion in Eqs. (2.11), (2.12), and (2.19).

In the long needle limit $\vartheta \nearrow 1$ one has $\tilde{\tau}_{i,h} \to 16[\Delta_{i,i}(0) - \Delta_{i,h}(0)]/\pi$ with $\Delta_{i,h}(0)$ given below Eq. (2.9) so that [53]

$$-(\partial/\partial a_N)F_\perp^{(i[h])}/k_BT \to [-3, -3, 61, 5]/(32a_<),$$
$$(i[h]) = [(O[O]), (+[+]), (-[+]), (+[O])]. \quad (3.9)$$

The behavior $\propto a_<^{-1}$ of the force per k_BT acting on the needle of infinite length $D = \infty$ follows easily [53] from

comparing its scaling dimension with that of the only remaining mesoscopic variable $a_<$. Unlike the expansion of the force for a small needle in which *fractional* powers such as $a_N^{-1}(D/a_N)^{1/8}$ may occur, the expansion around the long needle limit involves only contributions for which Eq. (3.9) is multiplied with positive *integer* powers of $a_</D \equiv \alpha$ (compare Eqs. (A7) and (A11), the relation between κ and $\bar{\vartheta}$ in Eq. (B22), and the relation $\bar{\vartheta}^2 = 4\alpha(1 + \alpha)/(1 + 2\alpha)^2$ which follows from Eq. (3.1)).

In the limit $\vartheta \nearrow 1$ the free energy per k_BT tends to

$$F_\perp^{(i[h])}/(k_BT) \equiv f_{i[h]}^\perp$$
$$\to ([-3, -3, 61, 5]/32) \ln(C_{i,h}/(1 - \vartheta)),$$
$$(i[h]) = [(O[O]), (+[+]), (-[+]), (+[O])], \quad (3.10)$$

where $1/(1 - \vartheta) \to D/(2a_<)$ in terms of $a_<$. Here $C_{i,h}$ are numbers, in particular $C_{O,O} = 2^{5/3}$ and $C_{+,O} = 2^{3/5}$ (see Eqs. (3.2) and (3.3)). This logarithmic behavior of $F_\perp^{(i[h])}/(k_BT)$ for the long *perpendicular* needle should be compared with the power law behavior $F_\parallel^{(i[h])}/(k_BT) \to \Delta_{i,h}D/a_<$ of the free energy for a long needle aligned at a small distance $a_<$ *parallel* to the boundary which is obtained by turning the perpendicular needle about that end which is closer to the boundary. For a particle of *circular* shape [22] with a radius R much larger than the distance $a_<$ between the closest points of the circle and the boundary, the interaction free energy $F^{(i[h])}/(k_BT) \to \pi\Delta_{i,h}(2R/a_<)^{1/2}$ exhibits, as expected intuitively, a power law exponent the value of which lies in between those corresponding to perpendicular and parallel needles. Unlike the long perpendicular needle, for the long parallel needle and the large circle the exact results of the interaction free energies quoted above are found already within the Derjaguin approximation and exhibit an amplitude proportional to $\Delta_{i,h}$ which depends on (i, h). For all three particles (the perpendicular and parallel needles as well as the circle) the particle-boundary interaction is attractive (repulsive) for $i = h$ ($i \neq h$).

Figure 3(a) shows a comparison between the exact result for $F_\perp^{(-[+])}/(k_BT) \equiv f_{-[+]}^\perp(\vartheta)$ which follows from Eq. (3.4) upon integration [50] and its "small needle approximation" ("sna") (compare Eqs. (B27) and (B33)). The approximation reproduces the exact result very well for $\vartheta < \vartheta_0$ with $0.3 \lesssim \vartheta_0 \lesssim 0.4$ while it fails for $\vartheta \gtrsim 0.6$ where it shows an unphysical maximum. For the *strip* situation $(-[+]j)$ with the center of the perpendicular needle at v_N, the question arises down to which proximity of the $+$ needle to the lower $-$ boundary of the strip one can expect the "small needle approximation" to be reasonably valid. Identifying the distance $a_N = D/(2\vartheta)$ in the half plane with the distance $W/2 - |v_N| \equiv W/2 + v_N$ in the strip suggests the approximation for $F_\perp^{(-[+]j)}$ to be valid if $|v_N|/W$ is smaller than $[1 - D/(W\vartheta_0)]/2$. For $0.3 \lesssim \vartheta_0 \lesssim 0.4$ and the value $D/W = 21/101$ used in our MC simulations (see, c.f., Subsec. V C) this rough argument predicts that $|v_N|/W$ should be kept smaller than
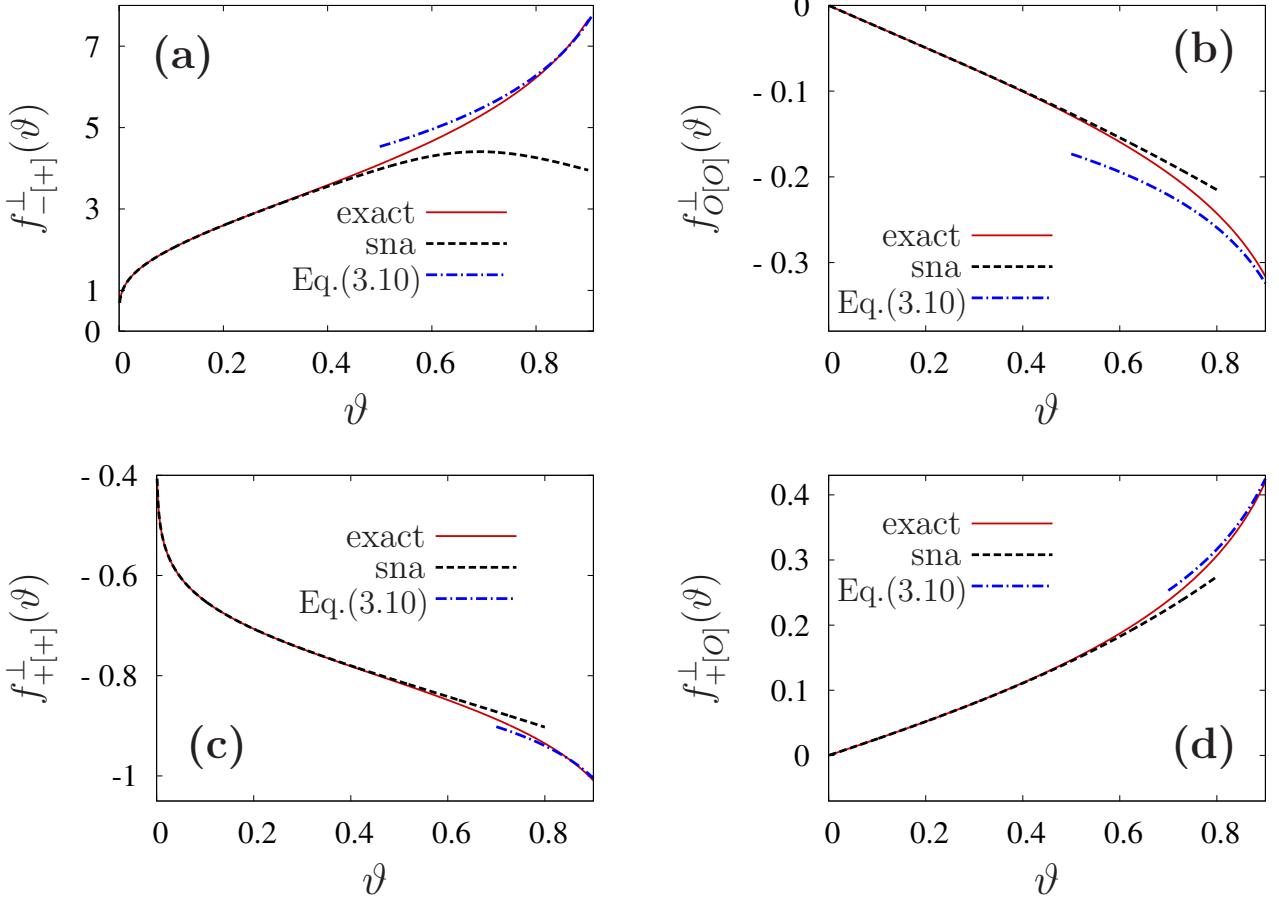
FIG. 3: Free energy cost per $k_B T$, $f_{i[h]}^\perp$, to transfer a needle of length D and universality class h from the unbounded plane (bulk) to the half plane, with an orientation which is perpendicular to the boundary of the half plane of universality class i. The dependence on $\vartheta = D/(2a_N)$, with a_N as the distance of the needle center from the boundary, is shown for various combinations $(i[h])$. The exact results for arbitrary $D/2 \leq a_N$ are compared with the "small needle approximation" ("sna", Eq. (B33)), which is valid for small ϑ, and with the long needle behavior for $\vartheta \to 1$ as given by Eq. (3.10). The interaction between the boundary and the needle is attractive (repulsive) for equal (different) universality classes $i = h$ ($i \neq h$) shown in (b) and (c) ((a) and (d)).

about 1/6 or 1/4, i.e., v_N should be kept rather close to the midline $v = 0$. For the anisotropy $\Delta F^{(-[+]j)}$ of the free energy of the needle in the strip there is even more uncertainty concerning the validity of the "sna" because the corresponding comparison for $F_\parallel^{(-[+])}$ is lacking, i.e., the counterpart of Fig. 3(a) for a needle parallel to the boundary of the half space is missing.

Figures 3(b)-(d) show the corresponding results for the free energies $k_B T f_{i[h]}^\perp$ with $(i,h) = (O,O)$, $(+,+)$, and $(+,O)$. For $i = h$ and $i \neq h$, $f_{i[h]}^\perp$ is negative and positive, respectively.

(ii) *Needle in infinitely long symmetric strip*

Here we consider a needle of universality class h and with parallel orientation $\parallel$ at the center line $v = 0$ of an infinitely long (i,i) strip of width W. We determine the free energy cost $F_\parallel \equiv F_\parallel^{(i[h]i)} = k_B T f_{i[h]i}^\parallel(\theta)$ and

the corresponding disjoining force $-(\partial/\partial W)F_\parallel^{(i[h]i)} = (k_B T/W)g_{i[h]i}^\parallel(\theta)$ between the two boundary lines of the strip upon inserting the needle from the bulk with parallel orientation. Here, the partial derivative is taken with the needle length D kept fixed. The disjoining force increases (decreases) if $g_{i[h]i}$ is positive (negative). The (i,h) symmetries of $F_\parallel^{(i[h]i)}$ are those of $\Delta_{i,h}$ as can be inferred from Eq. (3.15) below. The results depend on the length ratio [54]

$$\theta = \frac{\pi D}{W} \qquad (3.11)$$

and provide the crossover from the small needle behavior for $\theta \ll 1$, consistent with the "small needle expansion", to the long needle behavior for $\theta \gg 1$. In the latter case

one has

$$\frac{F_\parallel^{(i[h]i)}}{k_BT} \equiv f_{i[h]i}^\parallel \rightarrow D\left[2\frac{\Delta_{i,h}(0)}{(W/2)} - \frac{\Delta_{i,i}(0)}{W}\right]$$

$$= \theta[-1, -1, 31, 3]/16\,,$$

$$(i,h) = [(O,O),(+,+),(-,+),(+,O)] \quad (3.12)$$

because upon inserting a long parallel needle with its center at $u = v = 0$ transforms, within the interval $-D/2 < u < D/2$, the (i,i) strip of width W into two independent adjacent (i,h) strips of width $W/2$ each.

(iia) For $i = h = O$ the free energy to insert the needle from the bulk reads

$$\frac{F_\parallel^{(O[O]O)}}{k_BT} = -\frac{\theta}{8} + \frac{1}{16}\ln\frac{\sinh\theta}{\theta}\,. \quad (3.13)$$

(iib) For $i = +$, $h = O$ we find

$$\frac{F_\parallel^{(+[O]+)}}{k_BT} = \frac{\theta}{8} + \frac{1}{16}\ln\frac{\sinh\theta}{\theta} \quad (3.14)$$

which is Eq. (3.13) with θ replaced by $-\theta$. Equations (3.13) and (3.14) are derived in Appendix B1.

(iic) For *arbitrary* (i,h) we find (see Appendix B2)

$$-\frac{\partial}{\partial W}\frac{F_\parallel^{(i[h]i)}}{k_BT} = -\frac{\partial}{\partial W}\frac{F_\parallel^{(O[O]O)}}{k_BT} - \frac{1}{4W}\frac{\theta}{t}\tilde{\tau}_{i,h}(t)$$

$$\equiv \frac{1}{4W}\left\{-\frac{1}{4} + \theta\left[\frac{1}{24}\left(\frac{1}{t}+t\right) + \frac{1}{t}\rho_{i,h}(t)\right]\right\},$$

$$t \equiv \tanh(\theta/2)\,, \quad (3.15)$$

where $\tilde{\tau}_{i,h}(t)$ and $\rho_{i,h}(t)$ are the functions $\tilde{\tau}_{i,h}(\vartheta)$ and $\rho_{i,h}(\vartheta)$ from Eqs. (3.5) and (3.6), respectively, evaluated at $\vartheta = t$. Equations (3.13) and (3.14) as well as Eq. (3.15) are consistent with the "small needle expansion" for small θ (see Eqs. (B29)) and with Eq. (3.12) for large θ.

Figure 4 shows a comparison between the exact result for $F_\parallel^{(-[+]-)}/(k_BT) \equiv f_{-[+]-}^\parallel(\theta)$ which follows from Eq. (3.15) via integration [50] and its "small needle approximation" (compare Eqs. (5.4), (B30), (B32), and (B34)). For the value $\theta = 21\pi/101 = 0.653$ as used in our MC simulations (see Subsec. V C) there is good agreement. However, we have no such comparison for $F_\perp^{(i[h]i)}$.

All four possible independent free energies $k_BT f_{i[h]i}^\parallel(\theta)$ for needle insertion are collected in Fig. 5. They are negative (positive) for $i = h$ ($i \neq h$). In this double logarithmic plot the power laws as obtained for small θ from the "small needle expansion" and for large θ from the long needle expression (Eq. (3.12)) appear as straight lines.

(iii) *Periodic strip*

Finally we consider an infinitely long strip of width W with *periodic* boundary condition in v direction. In this
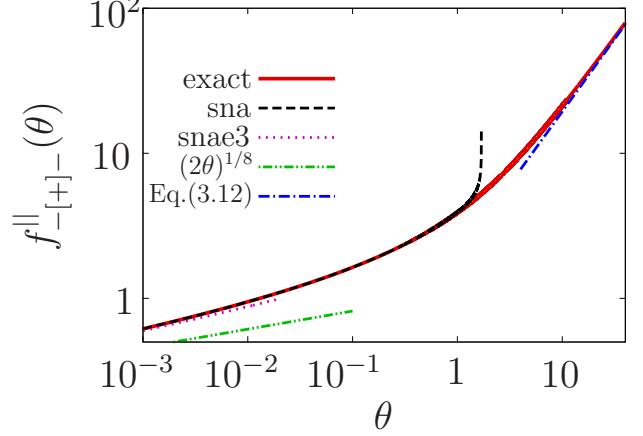

FIG. 4: Free energy cost per k_BT, $f_{-[+]-}^\parallel$, to remove a needle of universality class $+$ and length D from the bulk and insert it along the midline of an infinitely long strip with $(-,-)$ boundary conditions and width W as a function of $\theta = \pi D/W$ (see Ref. [50] and Eq. (3.15)). The exact result for arbitrary length ratio θ is compared with the "small needle approximation" ("sna", Eq. (B34)), valid for small θ, and with the long needle behavior according to Eq. (3.12). Also shown are the first term, $(2\theta)^{1/8}$, and the sum of the first three terms $(2\theta)^{1/8} + \theta^{1/4}/2^{3/4} + (2\theta)^{3/8}/3$, denoted as "snae3", in the expansion of $f_{-[+]-}^\parallel$ in terms of powers of θ for $\theta \ll 1$ (see Eqs. (B29) and (B32)). Expanding $f_{-[+]-}^\parallel$ proves to be less successful than the "sna" within which $\exp(-f_{-[+]-}^\parallel)$ is expanded and which agrees with the exact result up to $\theta \approx 1$. The first term (dash-double-dotted green line) approaches the exact result (full red line) for $\theta \rightarrow 0$ only very slowly.

case the free energy cost to insert a needle parallel to the strip reads (see Appendix B1)

$$\frac{F_\parallel}{k_BT} = \frac{1}{16}\ln\frac{\sinh\theta}{\theta}\,. \quad (3.16)$$

This result holds for any needle universality class $h = O, +, -$ and it is valid for an arbitrary ratio $\theta = \pi D/W$. Equation (3.16) should be compared with Eq. (3.13). For $\theta \gg 1$ the rhs of Eq. (3.16) tends to $\theta/16 = D\times[\Delta_{h,h}(0)-\Delta_P(0)]/W$. This is consistent with the periodic strip of width W being transformed, by inserting a parallel needle, to a (h,h) strip of width W within a u-interval of length D. Consistent with the "small needle expansion", for $\theta \ll 1$ the rhs of Eq. (3.16) tends to $\theta^2/96 + \mathcal{O}(\theta^4)$.

IV. FREE ENERGY ANISOTROPY FROM MONTE CARLO SIMULATIONS

The anisotropic shape of a bounded critical system induces orientation dependent properties for embedded non-spherical particles. In Sec. II the operator expansion has provided the asymptotic scaling properties for a "small" but "mesoscopic" particle in a "large" system. In
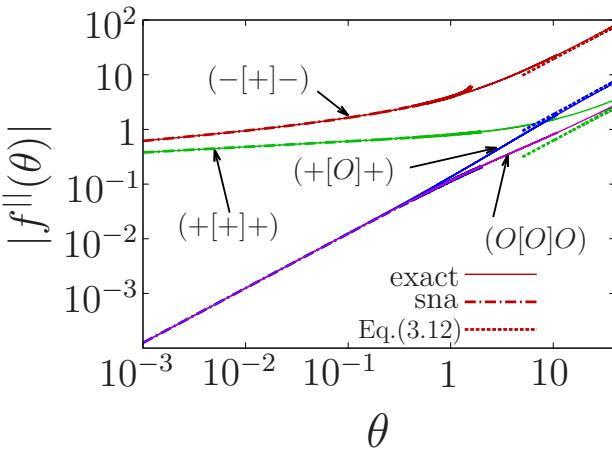
FIG. 5: Same as Fig. 4 for all four independent combinations $(i[h]i)$ of a needle of universality class h placed along the midline of an (i,i) strip as function of $\theta = \pi D/W$. Full, dash-dotted, and dotted lines correspond to the exact results, the "sna", and Eq. (3.12), respectively. For $h = i$ $(h \neq i)$ $f^{\parallel}_{i[h]i}$ is negative (positive), decreasing (increasing) with increasing θ, and implies a negative (positive) contribution $-\partial_W F^{(i[h]i)}_{\parallel} = (k_B T/W)\theta\partial_\theta f^{\parallel}_{i[h]i}$ to the disjoining force. Thus the attractive Casimir interaction (see Eq. (2.8)) with the negative universal disjoining force $-\partial_W k_B T \Phi^{(i,i)}_{ST} = \Delta_{i,i} k_B T L/W^2 = -(\pi/48)k_B T L/W^2$ between the (i,i) boundaries of the long strip without the needle becomes even more attractive (less attractive) due to the presence of the needle with $h = i$ $(h \neq i)$.

the present section we address the issue to which extent these asymptotic properties capture the actual behavior in specific critical model systems. Concerning the needles studied here, we want to check whether the asymptotic predictions of Sec. II for ΔF can already be observed within a lattice model with numerous, but not too many rows and columns so that the model is amenable to simulations. In this section we describe how to set up the corresponding Monte Carlo simulations and to calculate ΔF. In Sec. V we compare these simulation data with the corresponding analytic predictions. This allows us to judge both the achievements and the limitations of the "small particle approximation".

A. Model

For the simulation we use the lattice version of the Ising strip described in the Introduction and shown in Fig. 1. The implementation of the double periodic boundary conditions is obvious. Beyond that, here we describe in more detail strips with boundaries (i,j). In this case the lattice Hamiltonian $\mathcal{H}_{ST}$ for strips without a needle reads (see Sec. I):

$$\mathcal{H}_{ST}/\mathcal{J} = - \sum_{\langle u,v;u',v'\rangle} J_{u,v;u',v'}\, s_{u,v}\, s_{u',v'}$$

$$-\Lambda^{(1)}_i \sum_u s_{u,-(W+1)/2}\, s_{u,-(W-1)/2}$$

$$-\Lambda^{(1)}_j \sum_u s_{u,(W+1)/2}\, s_{u,(W-1)/2} \qquad (4.1)$$

with $\mathcal{J} > 0$ and $J_{u,v;u',v'} = 1$ for nearest neighbors (denoted by $\langle u,v;u',v'\rangle$) and zero otherwise. The fluctuating Ising spins $s = \pm 1$ reside on the vertices of the square lattice consisting of W rows and L columns with periodic boundary conditions in the u direction. The two last terms generate "ordinary" or "normal" $(+/-)$ boundaries near $v = -W/2$ and $v = W/2$ by means of fixed values $s_{u,-(W+1)/2} = s_{u,(W+1)/2} = 1$ for the spins in the two additional outside rows and by choosing independently $\Lambda^{(1)}_i$ and $\Lambda^{(1)}_j$ equal to 0 ("ordinary") or ± 1 $(+/-$ "normal"). This serves as a microscopic realization of all the pairs (i,j) of strip boundary types considered in Sec. II which exhaust all possible surface universality classes in $d = 2$ (up to the "extraordinary" boundary type [38, 44] corresponding to infinitely strong couplings between surface spins).

For reasons given in the Introduction and shown in Fig. 1, for "ordinary" ("normal") needles the number W of rows is taken to be even 2, 4, 6, ... (odd 1, 3, 5, ...) and the components of the lattice vertices u, v are half odd integers $\pm 1/2, \pm 3/2, \pm 5/2, ...$ (integers $0, \pm 1, \pm 2, ...$). The components $u = u_N$ and $v = v_N$ of the needle centers $\times$ are integers for both types of needles.

In order to be able to compare the Monte Carlo data with the results of Sec. II we consider the system at its bulk critical point T_c with $\mathcal{J}/(k_B T_c) = \frac{1}{2}\ln(\sqrt{2} + 1)$ where $\mathcal{J}$ is the coupling constant scaled out of $\mathcal{H}_{ST}$ (Eq. (4.1)).

Inserting a needle of class $h = O$ or $h = \pm$ into strips amounts to appropriately removing bonds or fixing spins in accordance with Fig. 1 via additional terms in the Hamiltonian. For given surface universality classes (i,j) of the strip, universality class h, needle length D, and the coordinate v_N of the center of the needle we introduce the notation

$$\mathcal{H} = \mathcal{H}_0 \equiv \mathcal{H}_{ST} + \mathcal{H}^{(h)}_{\perp} \qquad (4.2)$$

and

$$\mathcal{H} = \mathcal{H}_1 \equiv \mathcal{H}_{ST} + \mathcal{H}^{(h)}_{\parallel} \qquad (4.3)$$

for the total lattice Hamiltonian $\mathcal{H}$ corresponding to the needle being oriented perpendicular and parallel, respectively, to the u axis. The explicit forms of $\mathcal{H}^{(h)}_{\perp}$ and $\mathcal{H}^{(h)}_{\parallel}$ will be given in Eqs. (4.8), (4.9), and (4.11)-(4.18) below.

B. Numerical algorithm

1. Coupling parameter approach

We consider two systems with the same configurational space $\mathcal{C}$ (i.e., number and spatial connectivity of

spins) and with Hamiltonians $\mathcal{H}_0$ and $\mathcal{H}_1$ as given in Eqs. (4.2) and (4.3). The corresponding free energies are $F_{0,1} = -\frac{1}{\beta}\ln\sum_{\mathcal{C}}\exp(-\beta\mathcal{H}_{0,1})$; $\beta = 1/(k_B T)$ is the inverse thermal energy. We are interested in the free energy difference $\Delta F = F_1 - F_0$.

For the computation of this free energy difference we use the coupling parameter approach [55]. To this end we introduce the *cr*ossover Hamiltonian $\mathcal{H}_{\text{cr}}(\lambda)$ which depends on the coupling parameter λ,

$$\mathcal{H}_{\text{cr}}(\lambda) = \mathcal{H}_0 + \lambda\left(\mathcal{H}_1 - \mathcal{H}_0\right) = \mathcal{H}_0 + \lambda\Delta\mathcal{H}, \qquad (4.4)$$

with the Hamiltonian difference $\Delta\mathcal{H} = \mathcal{H}_1 - \mathcal{H}_0$ which in the present context is $\mathcal{H}_{\parallel}^{(h)} - \mathcal{H}_{\perp}^{(h)}$. The derivative of the corresponding *cr*ossover free energy $F_{\text{cr}}(\lambda) = -\frac{1}{\beta}\ln\sum_{\mathcal{C}}\exp(-\beta\mathcal{H}_{\text{cr}}(\lambda))$ with respect to the coupling parameter reads

$$\frac{dF_{\text{cr}}(\lambda)}{d\lambda} \equiv F'_{\text{cr}}(\lambda) = \frac{\sum_{\mathcal{C}}\Delta\mathcal{H}e^{-\beta\mathcal{H}_{\text{cr}}(\lambda)}}{\sum_{\mathcal{C}}e^{-\beta\mathcal{H}_{\text{cr}}(\lambda)}} = \langle\Delta\mathcal{H}\rangle_{\text{cr}}(\lambda),$$
$$(4.5)$$

where $\langle\Delta\mathcal{H}\rangle_{\text{cr}}(\lambda)$ is the Hamiltonian difference $\Delta\mathcal{H}$ averaged with respect to $\mathcal{H}_{\text{cr}}(\lambda)$. Therefore one can compute the free energy difference by integrating $\langle\Delta\mathcal{H}\rangle_{\text{cr}}$ with respect to λ:

$$\Delta F = F_1 - F_0 = \int_0^1 F'_{\text{cr}}(\lambda)d\lambda = \int_0^1 \langle\Delta\mathcal{H}\rangle_{\text{cr}}(\lambda)d\lambda. \quad (4.6)$$

For the forms of $\mathcal{H}_0$ and $\mathcal{H}_1$ given by Eqs. (4.2) and (4.3), respectively, one has

$$\Delta\mathcal{H} = \mathcal{H}_{\parallel}^{(h)} - \mathcal{H}_{\perp}^{(h)},$$
$$\mathcal{H}_{\text{cr}} \equiv \mathcal{H}_{\text{cr}}^{(h)} = \mathcal{H}_{\text{ST}} + (1-\lambda)\mathcal{H}_{\perp}^{(h)} + \lambda\mathcal{H}_{\parallel}^{(h)}. \quad (4.7)$$

2. Needle of broken bonds

Here we consider the combination $(i[O]j)$ corresponding to an "ordinary" needle which consists of an even number D of broken bonds in a strip with an even number W of rows. Figure 6 shows the example of a needle with $D = 4$ broken bonds in the center of an $L \times W = 6 \times 6$ strip. The Hamiltonians $\mathcal{H}_0$ and $\mathcal{H}_1$ for perpendicular and parallel needle orientation have the same form as the right hand side of Eq. (4.1) but with reduced interaction constants $J_{u,v;u',v'}$ which depend suitably on the coordinates (u,v) and (u',v') of nearest neighbor spins.

Choosing without restriction $u_N = 0$, the needle with center at $(0,v_N)$ is inserted in perpendicular orientation by "breaking", i.e., removing the D lattice bonds which at $v = v_N\pm 1/2$, $v_N\pm 3/2$, ..., $v_N\pm(D-1)/2$ extend from $u = -1/2$ to $u = 1/2$. This is accomplished by adding

$$\mathcal{H}_{\perp}^{(O)}/\mathcal{J} = \sum_{k=1}^{D} s_{-1/2,v_N-(D+1)/2+k}\, s_{1/2,v_N-(D+1)/2+k}$$
$$\equiv \sum_{\langle\text{inc.}\rangle} \qquad\qquad\qquad\qquad (4.8)$$
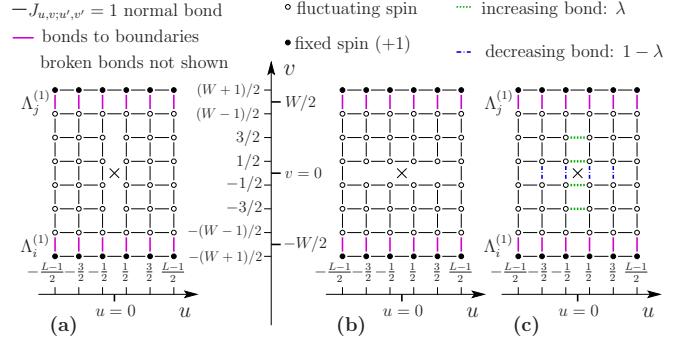
FIG. 6: Bond arrangements for a needle (O) of $D = 4$ *broken bonds* with center ($\times$) at $(u_N, v_N) = (0,0)$ at the midline $v = 0$ of a strip with $L = W = 6$: (a) for the perpendicular orientation of the needle with Hamiltonian $\mathcal{H}_0$; (b) for the parallel orientation of the needle with Hamiltonian $\mathcal{H}_1$; (c) for the crossover Hamiltonian $\mathcal{H}_{\text{cr}}^{(O)}(\lambda)$ which interpolates between (a) for $\lambda = 0$ and (b) for $\lambda = 1$. Bonds of strength $J = 1$ are indicated by thin black lines. Broken bonds ($J = 0$) are not shown. The bonds indicated by green dashed and blue dot-dashed lines have strengths λ and $1-\lambda$ which increase and decrease, respectively, as λ increases. As in Fig. 1 the fluctuating spins $s_{u,v} = \pm 1$ with $|v| \leq (W-1)/2$ are indicated by empty circles while the fixed spins $s_{u,\pm(W+1)/2} = 1$ in the two additional outside rows are indicated by full circles. The nearest neighbor bonds between fixed and fluctuating spins are indicated by thick magenta lines. For the lower and upper boundary i and j they have the strengths $\Lambda_i^{(1)}$ and $\Lambda_j^{(1)}$, respectively, where $\Lambda^{(1)}$ equals 0 for an O boundary and ± 1 for a $+/-$ boundary.

to the Hamiltonian $\mathcal{H}_{\text{ST}}/\mathcal{J}$ without needle (see Eq. (4.2)). Similarly for the parallel orientation of the needle one has to add

$$\mathcal{H}_{\parallel}^{(O)}/\mathcal{J} = \sum_{k=1}^{D} s_{-(D+1)/2+k,v_N-1/2}\, s_{-(D+1)/2+k,v_N+1/2}$$
$$\equiv \sum_{\langle\text{decr.}\rangle} \qquad\qquad\qquad\qquad (4.9)$$

so that $\Delta\mathcal{H} = \mathcal{H}_{\parallel}^{(O)} - \mathcal{H}_{\perp}^{(O)}$. Figures 6(a) and (b) illustrate these configurations for the special case $v_N = 0$.

The sums in Eqs. (4.8) and (4.9) have been characterized by subscripts $\langle\text{inc.}\rangle$ and $\langle\text{decr.}\rangle$ because in the crossover Hamiltonian following from Eq. (4.7),

$$\mathcal{H}_{\text{cr}}^{(O)}(\lambda) = \tilde{\mathcal{H}}^{(O)} - \lambda\mathcal{J}\sum_{\langle\text{inc.}\rangle} - (1-\lambda)\mathcal{J}\sum_{\langle\text{decr.}\rangle}, \quad (4.10)$$

they appear with a prefactor $-\lambda$ and $-(1-\lambda)$, respectively, representing sums of products of spins coupled by nearest neighbor bonds with strengths $\lambda\mathcal{J}$ and $(1-\lambda)\mathcal{J}$ which increase and decrease, respectively, as λ increases. Here $\tilde{\mathcal{H}}^{(O)} \equiv \mathcal{H}_{\text{ST}} + \mathcal{J}\sum_{\langle\text{inc.}\rangle} + \mathcal{J}\sum_{\langle\text{decr.}\rangle}$ equals $\mathcal{H}_{\text{ST}}$ in Eq. (4.1) but with both types of nearest neighbor bonds missing which are broken in the perpendicular or the

parallel orientation of the needle. This corresponds to Fig. 6(c) with both dashed and dash-dotted bonds removed (so that in $\tilde{\mathcal{H}}^{(O)}$ only those bonds of $\mathcal{H}_{ST}$ remain which are outside a hole with the shape of a cross). In $\mathcal{H}_{cr}^{(O)}(\lambda)$, however, the two types of missing bonds are replaced by the bonds of increasing and decreasing strength as illustrated in Fig. 6(c) by the green dashed and blue dash-dotted lines. This obviously leads to the crossover from the perpendicular to the parallel needle orientation as λ increases from 0 to 1.

On this basis, following the steps described by Eqs. (4.4)-(4.7) allows us to calculate $F_\parallel - F_\perp \equiv F_1 - F_0 = \Delta F$ for the combination $(i[O]j)$.

3. Needle of fixed spins

In this subsection we consider the lattice version of the case $(i[+]j)$ in which a needle consisting of an odd number D of spins fixed in the $+$ direction is embedded in a strip with an odd number W of rows. Figures 7(a) and

(a)

(b)
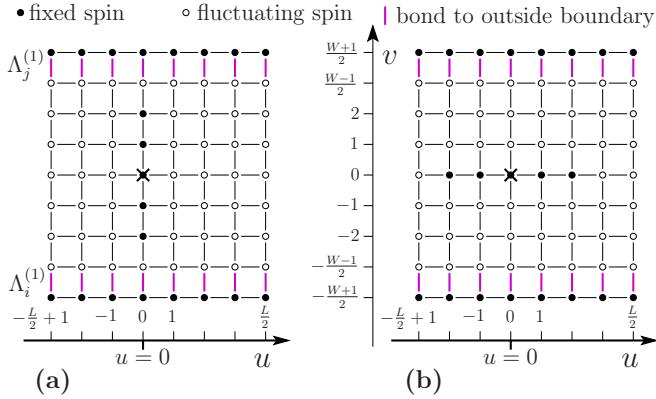
FIG. 7: Bond arrangements for a needle of $D = 5$ *spins fixed* in the $+$ direction with the needle center ($\times$) at $(u_N, v_N) = (0, 0)$ at the midline $v = 0$ of a strip with $L = 8$ and $W = 7$ for the perpendicular direction of the needle (a) and for the parallel direction of the needle (b). The strengths $\Lambda^{(1)}$ of the bonds near the strip boundaries are as explained in Fig. 6.

(b) show the example of a needle with $D = 5$ in the center of an $L \times W = 8 \times 7$ strip. The partition functions and free energies of these lattice models remain unchanged if the bonds between the fixed needle spins and their, in all, $2D+2$ fluctuating nearest neighbors are removed and these $2D+2$ neighbors are coupled instead with the bulk strength $\mathcal{J}$ to a *single* exterior spin $s_0 = +1$ which is kept fixed in the $+$ direction. The coupling to this single spin or to the D fixed spins has the same effect on the fluctuating spins, namely that of a magnetic field acting on the $2D + 2$ neighboring spins. Once this coupling to s_0 is in place, for the following it is convenient to replace each of the D fixed needle spins by a freely fluctuating spin, i.e., free of any couplings. This changes the free energy per $k_B T$ only by $D \ln 2$, independent of the orien-


(a)

(b)

(c)
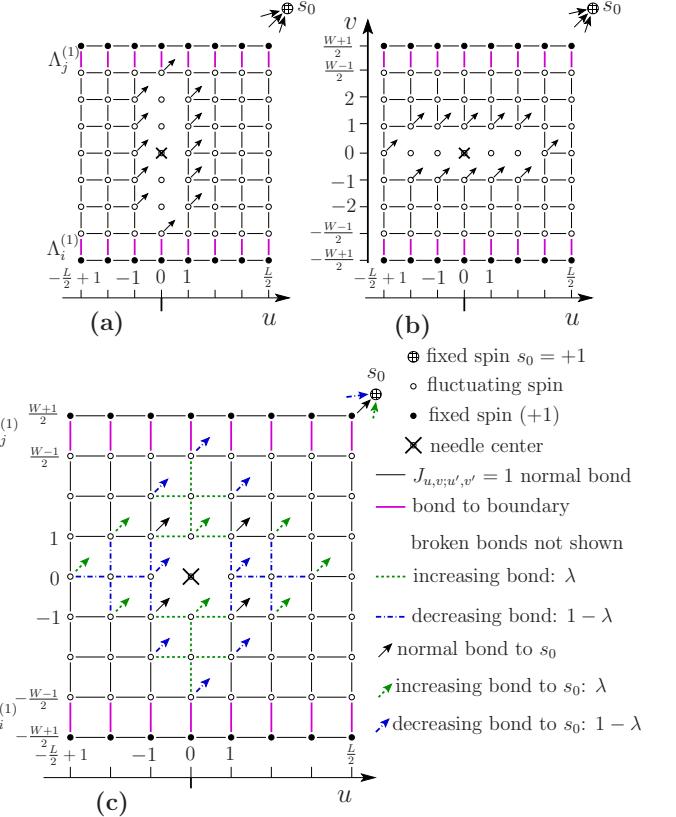
FIG. 8: (a) and (b) describe how to mimic the configurations discussed in Fig. 7 by means of couplings (north-east arrows) to a fixed external spin $s_0 = +1$; (c) shows the arrangement of bonds in the crossover Hamiltonian $\mathcal{H}_{cr}^{(+)}(\lambda)$ (see Eq. (4.19)) with their strengths indicated in the right margin. The arrangement reduces to that of (a) and (b) for $\lambda = 0$ and $\lambda = 1$, respectively. For further explanations see the main text.

tation of the needle and thus drops out of ΔF. For the above example discussed in Fig. 7 this alternative model is illustrated in Figs. 8(a) and (b), with the couplings to the external spin denoted by north-east arrows.

The corresponding additional terms in the Hamiltonian can be written as

$$\mathcal{H}_\perp^{(+)} = \sum_{\langle \text{zero} \rangle} + \widehat{\sum_{\langle \text{inc.} \rangle}} - \overset{(+)}{\sum_{\langle \text{one} \rangle}} - \overset{(+)}{\sum_{\langle \text{decr.} \rangle}} \qquad (4.11)$$

and

$$\mathcal{H}_\parallel^{(+)} = \sum_{\langle \text{zero} \rangle} + \widehat{\sum_{\langle \text{decr.} \rangle}} - \overset{(+)}{\sum_{\langle \text{one} \rangle}} - \overset{(+)}{\sum_{\langle \text{inc.} \rangle}} \qquad (4.12)$$

(so that $\Delta\mathcal{H} = \mathcal{H}_\parallel^{(+)} - \mathcal{H}_\perp^{(+)}$) where the sums

$$\sum_{\langle \text{zero} \rangle} = s_{0,v_N}(s_{-1,v_N} + s_{1,v_N} + s_{0,v_N+1} + s_{0,v_N-1}), \quad (4.13)$$

$$\widehat{\sum_{\langle \text{inc.} \rangle}} = \sum_{k=1}^{(D-1)/2} \Big[s_{0,v_N+k}(s_{-1,v_N+k} + s_{1,v_N+k}) \qquad (4.14)$$

$$+ s_{0,v_N-k}(s_{-1,v_N-k} + s_{1,v_N-k})$$

$$+ s_{0,v_N+k}s_{0,v_N+k+1} + s_{0,v_N-k}s_{0,v_N-k-1} \Big],$$

and

$$\widehat{\sum_{\langle \text{decr.} \rangle}} = \sum_{k=1}^{(D-1)/2} \Big[s_{k,v_N}(s_{k,v_N+1} + s_{k,v_N-1}) \qquad (4.15)$$

$$+ s_{-k,v_N}(s_{-k,v_N+1} + s_{-k,v_N-1})$$

$$+ s_{k,v_N}s_{k+1,v_N} + s_{-k,v_N}s_{-k-1,v_N} \Big]$$

contain products of nearest neighbor lattice spins while the sums

$$\overset{(+)}{\underset{\langle \text{one} \rangle}{\sum}} = s_{-1,v_N+1} + s_{1,v_N+1} + s_{-1,v_N-1} + s_{1,v_N-1}, \quad (4.16)$$

$$\overset{(+)}{\underset{\langle \text{decr.} \rangle}{\sum}} = s_{0,v_N+(D-1)/2+1} + s_{0,v_N-(D-1)/2-1}$$

$$+ s_{-1,v_N} + s_{1,v_N} \qquad (4.17)$$

$$+ \sum_{k=2}^{(D-1)/2} \Big[s_{-1,v_N+k} + s_{1,v_N+k} + s_{-1,v_N-k} + s_{1,v_N-k} \Big],$$

and

$$\overset{(+)}{\underset{\langle \text{inc.} \rangle}{\sum}} = s_{(D-1)/2+1,v_N} + s_{-(D-1)/2-1,v_N}$$

$$+ s_{0,v_N+1} + s_{0,v_N-1} \qquad (4.18)$$

$$+ \sum_{k=2}^{(D-1)/2} \Big[s_{k,v_N+1} + s_{k,v_N-1} + s_{-k,v_N+1} + s_{-k,v_N-1} \Big]$$

contain products of a lattice spin and the fixed external spin s_0 (which has the value $s_0 = +1$ and thus does not appear in Eqs. (4.16)-(4.18)). Here $\sum_{\langle \text{zero} \rangle}$ contains the products of the center ($\times$) spin of the needle with its four nearest neighbor spins which correspond to lattice bonds broken in both the perpendicular and parallel needle orientation (compare Figs. 8(a) and (b)). The products in $\widehat{\sum}_{\langle \text{inc.} \rangle}$ and $\widehat{\sum}_{\langle \text{decr.} \rangle}$ correspond to the remaining nearest neighbor bonds which are broken in the perpendicular and parallel needle orientation, respectively. The four terms in $\overset{(+)}{\underset{\langle \text{one} \rangle}{\sum}}$ correspond to the bonds between the external spin and those four lattice spins which are coupled to it in both the perpendicular and the parallel needle configuration (compare Figs. 8(a) and (b)). The sums

$\overset{(+)}{\underset{\langle \text{decr.} \rangle}{\sum}}$ and $\overset{(+)}{\underset{\langle \text{inc.} \rangle}{\sum}}$ contain the terms which correspond to the rest of the bonds to the external spin in the perpendicular and the parallel needle orientation, respectively.

As in the previous subsection the notation for the various sums reflects the modulus of their corresponding prefactors in the crossover Hamiltonian

$$\mathcal{H}_{\text{cr}}^{(+)}(\lambda) = \tilde{\mathcal{H}}^{(+)} - \lambda \mathcal{J} \widehat{\sum_{\langle \text{inc.} \rangle}} - (1-\lambda)\mathcal{J} \widehat{\sum_{\langle \text{decr.} \rangle}}$$

$$- \mathcal{J} \overset{(+)}{\underset{\langle \text{one} \rangle}{\sum}} - \lambda \mathcal{J} \overset{(+)}{\underset{\langle \text{inc.} \rangle}{\sum}} - (1-\lambda)\mathcal{J} \overset{(+)}{\underset{\langle \text{decr.} \rangle}{\sum}} . \quad (4.19)$$

The first term $\tilde{\mathcal{H}}^{(+)} \equiv \mathcal{H}_{\text{ST}} + \mathcal{J} \sum_{\langle \text{zero} \rangle} + \mathcal{J} \widehat{\sum}_{\langle \text{inc.} \rangle} + \mathcal{J} \widehat{\sum}_{\langle \text{decr.} \rangle}$ corresponds to a strip with a cross-shaped hole where the bonds belonging to $\sum_{\langle \text{zero} \rangle}$, $\widehat{\sum}_{\langle \text{inc.} \rangle}$, and $\widehat{\sum}_{\langle \text{decr.} \rangle}$ are missing (i.e., in Fig. 8(c) this means that the dashed and dash-dotted bonds and all the arrows are removed). In $\mathcal{H}_{\text{cr}}^{(+)}(\lambda)$ the contributions due to the two last types of bonds missing in $\tilde{\mathcal{H}}^{(+)}$, i.e., $\widehat{\sum}_{\langle \text{inc.} \rangle}$ and $\widehat{\sum}_{\langle \text{decr.} \rangle}$ carry the prefactors $-\lambda \mathcal{J}$ and $-(1-\lambda)\mathcal{J}$ of increasing and decreasing strengths , respectively. Moreover, bond contributions are added which couple the lattice spins contained in $\overset{(+)}{\underset{\langle \text{one} \rangle}{\sum}}$, $\overset{(+)}{\underset{\langle \text{inc.} \rangle}{\sum}}$, and $\overset{(+)}{\underset{\langle \text{decr.} \rangle}{\sum}}$ with strengths 1, λ, and $1 - \lambda$, respectively, to the external spin $s_0 = 1$. For $L = 8$, $W = 7$, $D = 5$, and the needle center $\times$ at $v_N = 0$ at the midline of the strip, the various bond strengths in $\mathcal{H}_{\text{cr}}^{(+)}(\lambda)$ are shown in Fig. 8(c) which clearly illustrates the crossover from the perpendicular to the parallel needle orientation considered in Figs. 8(a) and 8(b) as λ increases from 0 to 1.

4.   Details of the numerical implementation

For the sequential generation of system configurations we have used the hybrid Monte Carlo method [56]. One step consists of updating a Wolff cluster [57] followed by $L \times W/4$ attempts of Metropolis updates [58] of randomly chosen spins and of additional $(D+3)^2$ updates of randomly chosen spins in the square of size $(D+3) \times (D+3)$ with the center at position $(0, v_N)$.

In order to determine the dependence of the free energy on v_N we have used system sizes 1000×100 and 1000×101 for $(i[O]j)$ and $(i[+]j)$ needles, respectively. For thermalization we have used 1.5×10^7 MC steps, followed by the computation of the thermal average using 8×10^7 MC steps. These latter MC steps have been split into 16 intervals which facilitates to estimate the numerical inaccuracy.

In order to determine the aspect ratio dependence of the free energies we have used various numbers of MC

$W = 100$ and $D = 10$ and 20. The data for the "normal" needle of "fixed spins" stem from systems with $W = 101$ and $D = 11$ as well as $D = 21$. The data for $D = 20$ and $D = 21$ are in rather good agreement with the expression $[\Delta F_l/(k_B T)]/(D/W)^2$, as predicted according to Eq. (5.1) and Appendix A 1 for the leading order contribution $\propto D^2$, shown as the red dash-dotted line. The data for the "ordinary" needle are indeed slightly larger than those for the "normal" needle, as predicted by the next-to-leading order contribution $\propto D^3$ in Eq. (5.1). The stronger deviations of the data for $D = 10$ and $D = 11$ from the analytic approximation presumably indicate that these smaller needle lengths lie outside the mesoscopic scaling region required [24] for the validity of Eq. (5.1).

B. Dependence of the free energy anisotropy on the spatial position of needles in strips.

In strips with boundaries ΔF depends on the position v_N of the needle in the strip. Here we consider strips of infinite length L, either with arbitrary boundaries (i, j) and containing an "ordinary" needle or with boundaries (O, O) and containing a "normal" needle. In all these cases $\Delta F \simeq \Delta F_l + \Delta F_{nl}$ is predicted to have the form given by Eqs. (2.16)-(2.18).

Ordinary needles

While ΔF_l does not depend on v_N and is given by Eq. (2.17) with $\Delta_{i,j}$ given below Eq. (2.9), in the cases $(i[O]j)$ one has

$$\frac{\Delta F_{nl}}{k_B T} = \frac{1}{256}\left(\frac{\pi D}{W}\right)^3 g_{i,j} \qquad (5.2)$$

which depends on v_N via the following simple expressions for $g_{i,j}$:

$$g_{O,O} = 3(\cos V)^{-3} - (5/3)(\cos V)^{-1}$$
$$g_{+,+} = -g_{O,O}$$
$$g_{+,O} = -g_{O,+} = (\tan V)[3(\cos V)^{-2} + (1/3)]$$
$$g_{+,-} = g_{-,+} = -[3(\cos V)^{-3} +$$
$$+ (7/3)((\cos V)^{-1} - 4\cos V)] \quad (5.3)$$

with $V = \pi v_N/W$. They follow upon inserting $f_\epsilon^{(i,j)}$ from Eq. (A14) and $\mathcal{A}_\epsilon^{(h)} \equiv \mathcal{A}_\epsilon^{(O)} = 1/2$ (see Eq. (2.5)) into Eq. (2.18).

Figure 10 compares our simulation data for the cases $(i[O]j)$ with the corresponding analytic predictions for various positions v_N of the needle and for various boundary conditions (i, j) of the strip. The plots show the data for $[(\Delta F - \Delta F_l)/(k_B T)]/(D/W)^2$ with ΔF obtained from a system with $L = 1000$, $W = 100$, and $D = 20$. The comparison with $[\Delta F_{nl}/(k_B T)]/(D/W)^2 \equiv c_{i,j}$ following from Eqs. (5.2) and (5.3) and shown by lines is very favorable (i.e., ΔF is captured well by $\Delta F_l + \Delta F_{nl}$), except
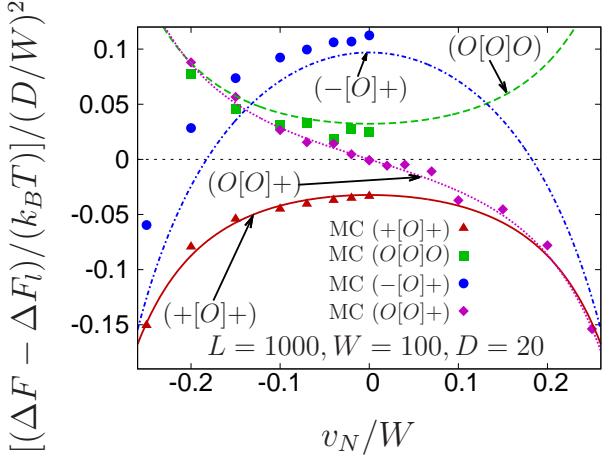
FIG. 10: Quasi-torque ΔF acting on a small mesoscopic "ordinary" needle O in a long strip with boundaries (i, j) corresponding to the cases $(i[O]j)$. This plot shows its dependence on the position v_N of the needle in the strip and on the boundary conditions (i, j). The lines are suitably normalized expressions c_{ij} (see Eqs. (5.2) and (5.3) and the text below the latter one) for ΔF_{nl} which, according to Eq. (5.3), are symmetric around $v_N/W = 0$ for $(i, j) = (O, O)$, $(+, +)$, and $(-, +)$ but antisymmetric for $(i, j) = (O, +)$. In order to obtain the numerical data we have computed ΔF by means of the coupling parameter approach (Sec. IV) and then have subtracted the analytic expression (2.17) for ΔF_l. There is very favorable agreement of the simulation data, which correspond to $W/L = 0.1$, with the analytic predictions for $W/L = 0$. The case $(-[O]+)$ is exceptional in that for it the agreement is only fair, i.e., in this case there are sizeable corrections to $\Delta F = \Delta F_l + \Delta F_{nl}$ beyond ΔF_{nl}. The statistical error bars are comparable with the symbol sizes and therefore they are omitted.

for the case $(-[O]+)$ in which it is only fair. According to Eqs. (5.2) and (5.3) one has $c_{i,j} = (\pi^3/256)(D/W)g_{i,j}$.

In order to visualize the approach of the limit of infinite strip length $L = \infty$, Figs. 11 and 12 show [60] the dependence of the quasi-torque on the aspect ratio W/L for needles of length $D = 10$ or $D = 20$ with their center $v_N = 0$ at the midpoint of a strip of width $W = 100$. The cases $(O[O]+)$ and $(O[O]-)$ should lead to the same ΔF, due to the $(+ \leftrightarrow -)$ symmetry [34] of the Ising model, and ΔF_{nl} should vanish for $v_N = 0$, due to Eq. (2.18) and Ref. [48]. These properties are reflected rather well by the data in Fig. 11 for $D = 20$ (shown as squares and diamonds) which are close to the values of $[\Delta F_l/(k_B T)]/(D/W)^2$, equal to $-\pi^2/96$ for $W/L = 0$ (shown as the horizontal straight line) and about 5% smaller for $W/L = 1/2$. Here we discard the data for $W/L \leq 0.1$ which carry large error bars. This should be compared with the case $(O[O]O)$ discussed in Fig. 12 where in a strip of width $W = 100$ the data for the needle of length $D = 20$ (shown by squares) attain much closer the asymptotic value $(\pi^2/192)(1 + 20\pi/100)$ of $[(\Delta F_l + \Delta F_{nl})/(k_B T)]/(D/W)^2$ predicted for $v_N = 0$ and $L = \infty$ (shown as the uppermost straight line) as L
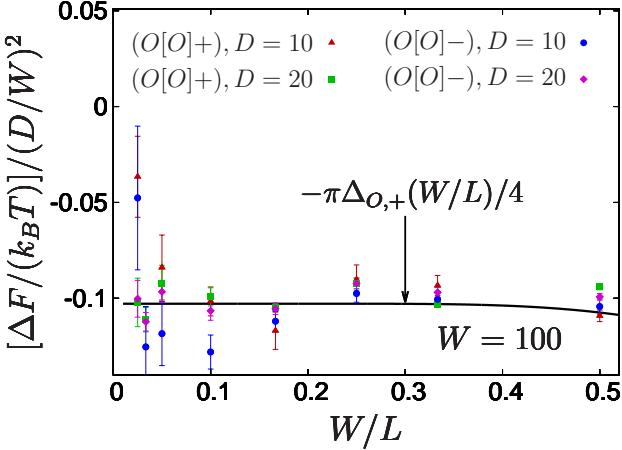
FIG. 11: Dependence of the quasi-torque ΔF on the aspect ratio W/L of the strip for $(O[O]+)$ and $(O[O]-)$ boundary conditions with the needle at the strip center $v_N = 0$. In these cases the next-to-leading contribution ΔF_{nl} vanishes [48] for arbitrary W/L and the simulation data for $D = 20$ (squares and diamonds) are indeed close to the values given by $-\pi\Delta_{O,+}(W/L)/4$ (full black line) corresponding to the leading contribution ΔF_l which are $-\pi^2/96$ for $W/L = 0$ and about 5 percent smaller for $W/L = 1/2$ (see Eqs. (A5), (A7), and (A9)). This decrease is too weak to be reflected by the present simulation data. Due to the inherent $(+ \leftrightarrow -)$ symmetry, one has $\Delta F^{(O[O]+)} = \Delta F^{(O[O]-)}$ for *arbitrary* values of D, v_N, W, and L. This exact identity is embodied in the form of the corresponding lattice Hamiltonians $\Delta\mathcal{H}$ and $\mathcal{H}_{cr}(\lambda)$ in Sec. IV. However, the results for the thermal average $\langle\Delta\mathcal{H}\rangle_{cr}(\lambda)$ and its integral ΔF in Eq. (4.6), calculated by means of the statistical Monte Carlo method, violate this identity within the numerical inaccuracy. Note that the ensuing deviations in the above data are of tolerable size, at least for the larger value of D.

increases, i.e., as W/L becomes smaller.

Normal needles in strips without broken symmetry

Now we consider the (equivalent) cases $(O[+]O)$ and $(O[-]O)$ of a "normal" needle with $h = +$ or $-$ in an (O, O) strip. Figure 13 shows data [60] for $[\Delta F/(k_B T)]/(D/W)^2$ for such a needle of length $D = 21$ at various positions v_N in a strip with $L = 1000$ and $W = 101$. They compare favorably with the corresponding analytic expression $-(\pi/4)\Delta_{O,O} + (\pi^3/256)(D/W)(-g_{O,O})$ for $[(\Delta F_l + \Delta F_{nl})/(k_B T)]/(D/W)^2$ with $L = \infty$, which is shown as dashed line. This expression follows from Eqs. (2.16)-(2.18) by repeating analogously the line of arguments leading to Eqs. (5.2) and (5.3). Here the sign in front of $g_{O,O}$ differs from that in Eq. (5.2) for the "ordinary" needle because $\mathcal{A}_\epsilon^{(+)} = \mathcal{A}_\epsilon^{(-)} = -\mathcal{A}_\epsilon^{(O)}$ (Eq. (2.5)). In strips of infinite length L the pseudo-torques $\Delta F(v_N)$ for the present case $(O[+]O)$ and for the case $(+[O]+)$ considered above are *identical*. This follows from a duality argument similar to the one in Ref. [44], is in agreement with the expression $\Delta F_l + \Delta F_{nl}$ in Eqs. (2.16)-(2.18), and is quite well reflected by the simulation data in Figs. 10 and 13. Concerning the aspect ratio dependence
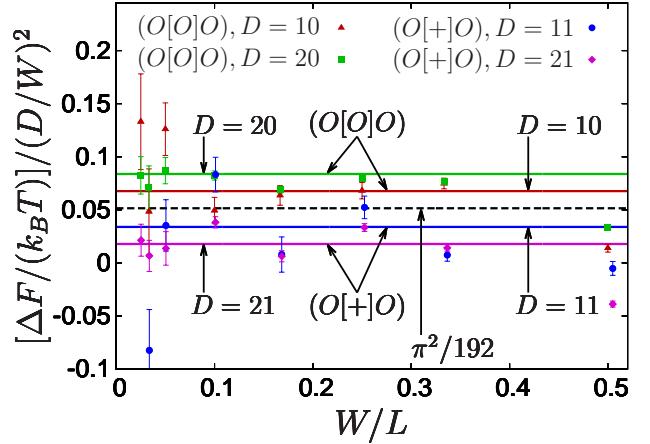
FIG. 12: Similar as Fig. 11 but for the cases $(O[O]O)$ and $(O[+]O)$ in which, for $L = \infty$, $[(\Delta F_l+\Delta F_{nl})/(k_B T)]/(D/W)^2$ equals $(\pi^2/192)[1+\pi D/W]$ and $(\pi^2/192)[1-\pi D/W]$, respectively, so that the leading contributions (dashed line) are the same. For small W/L the simulation data for $D = 20, W = 100$ and $D = 21, W = 101$ (green squares and magenta diamonds) are indeed close to the corresponding uppermost and lowest horizontal line, respectively.
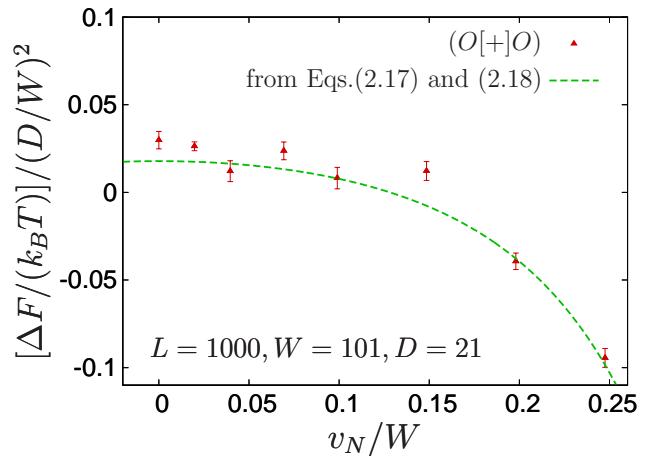
FIG. 13: Dependence of the quasi-torque ΔF on the position v_N of the needle in the $(O[+]O)$ case. The simulation data (triangles) agree well with the analytic prediction (dashed line) given by $\Delta F_l + \Delta F_{nl}$ (see the main text).

dence, for $W/L \le 0.1$ the data for the case $(O[+]O)$ of a "normal" needle with $v_N = 0$ and $D = 21$ (shown by diamonds in Fig. 12) have the tendency to approach the predicted limiting value $(\pi^2/192)(1-21\pi/101)$ (indicated in Fig. 12 by the lowest horizontal straight line).

C. "Normal" needles in strips with broken symmetry

In this subsection we consider a "normal" needle with $h = +$ embedded in strips with at least one "normal"
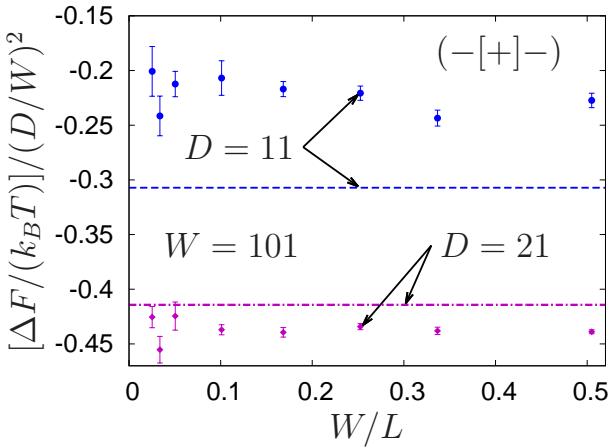
FIG. 14: Quasi-torque ΔF acting on a $+$ needle in the center of a $(-,-)$ strip. We show simulation data for needles of length $D = 11$ and 21 in strips of width $W = 101$ and of various lengths L. The data for $D = 21$ (diamonds) agree quite well with the "sna" prediction -0.4143 (dash-dotted line) for a strip of infinite length as explained in the first two paragraphs of Subsec. V C. For the smaller needle of length $D = 11$ there is a significant discrepancy between the simulation data and the "sna" prediction -0.3072 (dashed line) for a strip of infinite length.

boundary. These are the boundary conditions $(i,j) = [(+,+),(-,-),(+,-),(+,O),(-,O)]$ for which the order parameter profiles $\langle\phi\rangle_{ST} = W^{-1/8}f_\phi^{(i,j)}$ in Eq. (2.7) are nonvanishing and ζ_I in Eq. (2.13) contains a contribution $\propto D^{1/8}$. In these cases we do not compare our simulation data with the expanded analytic form of ΔF, because confining this expansion to the two leading powers of D, as in Eq. (2.16), is expected to be insufficient for reaching agreement with presently accessible simulation data. As explained there, we rather set out to compare the simulation data with the full expression "sna" of the "small needle approximation" following from Eqs. (2.10)-(2.15). While we disregard the terms of order D^4 denoted by the ellipses [41] in Eqs. (2.13) and (2.14), we leave the logarithm in Eq. (2.15) unexpanded.

We illustrate this point for the case $(-[+]-)$, i.e., a $+$ needle embedded in a $(-,-)$ strip. Figure 14 shows[60] that $[\Delta F/(k_BT)]/(D/W)^2$ as obtained from simulations for a needle (with $D = 21$ and located in the center of a strip with $W = 101$) agrees, for smaller aspect ratios W/L, quite well with the prediction -0.4143 for $L = \infty$ (see the diamonds and the dash-dotted bottom line in Fig. 14). The prediction follows by inserting the present value $\theta = 21\pi/101 = 0.653$ of $\theta \equiv \pi D/W$ into the "sna" expression $\Delta F/(k_BT) = -\ln(Z_\parallel/Z_\perp)$ where

$$
\begin{aligned}
Z_{\parallel,\perp} = \ & 1 \ -(2\theta)^{1/8} - 2^{-6+1/8}\theta^{17/8} + 2^{-3}\theta + 2^{-9}\theta^3 \\
& + \ (1,-1) \times [-2^{-7}(1/3)\theta^2 \\
& \qquad\qquad +2^{-6+1/8}(1/3)\theta^{17/8} - 2^{-10}3\theta^3], \quad (5.4)
\end{aligned}
$$

see Eqs. (2.5) and (2.12)-(2.14) with the value $\Delta_{-,-} =$

$-\pi/48$ taken from below Eq. (2.9) as well as Eqs. (A14) and (A15). For this value of θ the validity of the "sna" is confirmed by Fig. 4, as far as the contribution $F_\parallel$ to ΔF is concerned (compare the discussion in the paragraph below Eq. (3.15)). This should be contrasted with the prediction -0.0017 (as compared with -0.4143, see above) which would follow from ΔF being truncated after the leading and the next-to-leading order in D, i.e., from $(\Delta F_l + \Delta F_{nl})/k_BT = [(2\theta)^2 - (2\theta)^{17/8}]/(3 \times 2^8)$ (by using again Eq. (5.4)) and which would disagree with the simulation data by a factor of about 250.

The reasonable agreement between the simulation data for $D = 21$ and the "sna" persists for the dependence on the needle position v_N shown as the squares and the green dashed line in Fig. 15, provided $|v_N|/W$ remains small.

However, for $|v_N|/W \gtrsim 0.15$ an even qualitative deviation develops in that the analytic approximation predicts a point of inflection and a minimum which is not supported by the simulation data. We attribute this failure to inadequacies of this approximation near the strip boundary which have been discussed in detail for $F_\perp$ in the half plane (see the paragraph in Sec. III addressing Fig. 3(a)). In particular the unphysical minimum of the green dashed line in Fig. 15 is related to the maximum of the "sna" result shown in Fig. 3(a).

This dependence on v_N/W is shown in Fig. 15 also for the other cases $(-[+]O), (+[+]O), (+[+]-)$, and $(+[+]+)$ of a $+$ needle embedded in strips with at least one "normal" boundary. Also in these cases the dependences of the data on v_N/W are reproduced reasonably well by the "sna".

VI. SUMMARY AND CONCLUDING REMARKS

A critical solvent such as a binary liquid mixture at its continuous demixing transition induces a long-ranged, so-called critical Casimir interaction between immersed particles which is universal on mesoscopic length scales. For *nonspherical* particles the interaction depends not only on their sizes and distances among each other but also on their shapes and mutual orientations. We have studied a critical system belonging to the Ising bulk universality class in two spatial dimensions and particles of needle shape.

As described in the Introduction we have considered Ising strips at the bulk critical point with an embedded needle which is oriented either parallel or perpendicular to the symmetry axis of the strips. For such systems our analysis benefits from the wealth of knowledge accumulated for the two-dimensional Ising model at criticality and the comparative ease to implement a needle along a row or column of the square lattice. The corresponding effective interaction between the needle and the two strip boundaries is probably the simplest example to check by Monte Carlo simulations the range of validity of asymptotic analytic predictions for the orienta-

tion dependence of critical Casimir interactions between nonspherical mesoscopic particles which go beyond the Derjaguin approximation.

In Sec. IV and Figs. 1, 6, 7, and 8 we explain how to implement in the lattice model boundary properties at the two confining surfaces of the strip and for the needle, which locally induce one of the two demixing bulk phases ("normal" surface universality classes $+$ (or $-$)) or induce disorder and suppress demixing ("ordinary" surface class O). The geometrical features of the corresponding continuum description are explained in Fig. 2.

Primarily, we analyze the free energy $\Delta F = F_\parallel - F_\perp$ required at bulk criticality to turn the needle from an alignment perpendicular to the strip (with free energy $F_\perp$) to parallel alignment (with free energy $F_\parallel$). Thus one has $\Delta F > 0$ and $\Delta F < 0$ if the needle prefers the perpendicular and parallel alignment, respectively. ΔF depends on the length D of the needle, the width W and length L of the strip, the distance v_N of the needle center from the midline of the strip, and the surface universality classes h of the needle and (i, j) of the two boundaries of the strip. Here we consider needles of *small* mesoscopic length D for which predictions are available from the so-called "small needle expansion" explained in Sec. II.

Before presenting below an itemized summary of the quantitative comparison with the simulations we point out a few qualitative observations. For the needle it is advantageous to reside in a spatial region and take an orientation which suits its boundary condition.

(i) First, consider a needle of universality class h in a *half plane* with the boundary belonging to surface universality class i. The needle will prefer the vicinity of this boundary if $i = h$. Since in the case $i = +$ ($i = O$) the boundary-induced order (disorder) increases upon approaching the boundary - as described, according to Eq. (2.5), by the concomitant increasing density profiles of the order parameter (of the energy) in the half plane without needle - this leads to an attractive force between needle and boundary. Since both increases are stronger than linear, for a fixed needle center in both cases the needle will adopt an orientation perpendicular to the boundary of the same class. Likewise, for different universality classes $i \neq h$ of the needle and the boundary the force will be repulsive and for a fixed center the needle will orient parallel to the boundary [13]. These orientational preferences depend on the needle position, increasing and decreasing, respectively, with decreasing and increasing distance a_N of the needle center from the boundary.

(ii) In a *strip* there is an additional qualitative effect in that there is a contribution to the orientational preference of the needle which is *independent* of its position v_N in the strip but depends on the combination (i, j) of surface universality classes of the two strip boundaries. In a long strip this contribution favors an alignment of the needle perpendicular (parallel) to the boundaries if they belong to the same (different) universality class $i = j$ ($i \neq j$). For the double periodic strip it favors an alignment perpendicular to the longer axis.

This is reminiscent of - and related to - a well known corresponding anisotropy [59] of the two-point averages $\langle \mathcal{O}(\mathbf{r} - \mathbf{s}/2)\mathcal{O}(\mathbf{r} + \mathbf{s}/2)\rangle_{\mathrm{ST}}$ in the strip of the densities $\mathcal{O} = \phi$ of the order parameter and $\mathcal{O} = \epsilon$ of the energy. For small mesoscopic distances $|\mathbf{s}|$ the anisotropy causes the two-point averages to be larger for $\mathbf{s}$ perpendicular (parallel) to the two strip boundaries if $i = j$ ($i \neq j$) and for $\mathbf{s}$ perpendicular to the longer axis of the double periodic strip.

All of these expectations are confirmed and further refined by the quantitative predictions of the "small needle expansion". It predicts, in particular, that the anisotropy ΔF due to [61] the aforementioned effect (ii) depends, apart from the boundary classes (i, j) of the strip, only on the length and not [40] on the universality class ($h = +$, $-$, or O) of the small mesoscopic needle.

In the following three blocks A, B, and C we list our main results.

(A) We have demonstrated that the quantitative predictions of Sec. II for the rich structure of the orientation-dependent interaction of non-spherical particles with a "small mesoscopic size" can actually be observed in a lattice model. This is a nontrivial result in view of a twofold size condition: the particle size being small compared with other geometric features and being large on the scale of the lattice constant. Our Monte Carlo simulations with needle lengths of about 20 lattice constants [27] have the potential to closely approach the asymptotic regime of the "small mesoscopic needle", leading to results for ΔF which agree quite well with the analytic predictions, without adjusting any parameter. At the same time, the parameter range in which there is good agreement provides a (conservative) estimate for the range of validity of the "small needle approximation" ("sna"), which is a truncated form of the systematic expansion for the universal quasi-torque ΔF in terms of the needle size.

A1. For a strip with double periodic boundary conditions, for which the aforementioned effect (i) is absent, our data for ΔF reproduce, for the larger needle lengths $D = 20, 21$, quite well the predicted dependence of ΔF on the aspect ratio W/L of the strip and the predicted independence of ΔF of the universality classes $h = O$ and $h = +$ of the needle, in leading order (see Fig. 9 and the discussion in Subsec. V A).

A2. In strips with actual boundaries, effects of both type (i) and (ii) are present and the former ones lead to a dependence of $F_\parallel$, $F_\perp$, and ΔF on the position v_N of the needle center within the strip. Here the analytic predictions hold for strips of infinite length $L = \infty$ and Figs. 11, 12, and 14 show the dependence of the simulation data on the aspect ratio W/L of the strip.

A2a. For the five possible and relevant combinations $(i[h]j) = (O[O]O)$, $(+[O]+)$, $(-[O]+)$, $(O[O]+)$, and $(O[+]O)$ of universality classes of the two
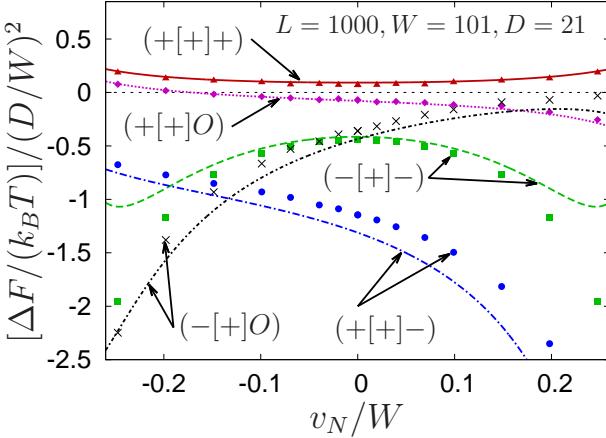
FIG. 15: Quasi-torque ΔF acting on a small mesoscopic "normal" needle $+$ in a long strip in which one or both boundaries break the Ising symmetry. We show the dependences of ΔF on the position v_N of the needle in the strip and on the boundary conditions (i,j) of the strip. There is reasonable agreement of the simulation data for $W/L = 0.1$ with the analytic predictions of the "small needle approximation" for $W/L = 0$ which are discussed in the first paragraph of Subsec. V C. For the case $(-[+]-)$ the "sna" can be trusted only for $|v_N|/W$ smaller than ≈ 0.15 (see the discussion in the last but one paragraph of Subsec. V C). The statistical error of the simulation data is comparable with the symbol sizes.

boundaries of the strip and of the embedded needle, for which the expansion in Eqs. (2.16)-(2.18) of ΔF in terms of powers of D is appropriate, the dependence on v_N of our data for ΔF is discussed in Subsec. V B. In Figs. 10 and 13 this dependence is compared with the approximate analytic predictions. There is fair agreement for the case $(-[O]+)$ while in the four other cases the agreement is very good.

In the case $(O[O]+)$, due to effect (i) one has $\Delta F(v_N) > 0$ and $\Delta F(v_N) < 0$ near the O and $+$ boundary, respectively, so that the needle prefers the perpendicular and parallel orientation, respectively. Since effect (ii) for unequal strip boundaries turns the needle parallel to the strip, the range of v_N values allowing for parallel orientation is the larger part of the accessible values of v_N, i.e., the point v_N where ΔF changes sign is closer to the O boundary.

In the strip of infinite length $L = \infty$ duality arguments [38, 44] predict for the cases $(+[O]+)$ and $(O[+]O)$ the same expression for $\Delta F(v_N)$ which within the "sna" (Eqs. (2.16)-(2.18)) is visualized as the full line in Fig. 10 and as the dashed line in Fig. 13. It predicts that in this case the needle prefers the orientation perpendicular to the strip for small $|v_N|$ where effect (ii) prevails so that $\Delta F > 0$, while for larger $|v_N|$ where effect

(i) prevails it prefers the parallel orientation with $\Delta F < 0$. The good agreement with the data in Figs. 10 and 13 tells again that within our lattice model one can access the scaling region and thus capture the corresponding universal small particle behavior.

A2b. Unlike the combinations considered above (in A2a.) the five combinations $(i[h]j) = (+[+]+), (-[+]-), (+[+]-), (+[+]O), (-[+]O)$ discussed in Subsec. V C involve a needle which at T_c is subject to the order parameter profile induced by the strip boundaries (i,j) via its nonvanishing amplitude $\mathcal{A}_\phi^{(h)}$ (see Eqs. (2.10)-(2.14)). This leads to a contribution to the partition function $\propto D^{1/8}$. For the comparison with the simulation data for ΔF, in these five cases the corresponding "small needle approximation" should not be implemented by directly expanding ΔF in terms of powers of D but by expanding the corresponding partition functions (see the remarks above Eq. (2.16) and in the first paragraph of Subsec. V C). The comparison of the analytical predictions for these cases with the corresponding MC data is shown in Fig. 15. The orientation preferred by the needle (i.e., the sign of ΔF) is in conformance with [62] the qualitative observation (i); also quantitatively the MC data agree quite well with the predictions. According to Fig. 15, in the case $(-[+]-)$, however, the good agreement for small values of $|v_N|/W$ does not extend beyond $|v_N|/W \approx 0.15$. In this case the expected breakdown of the "small needle approximation" near strip boundaries starts already rather close to the strip center producing an unphysical minimum of $\Delta F(v_N)$ at $|v_N|/W \approx 0.25$.

(B) We have investigated the effective interaction between the needle and the boundaries also for needles of *arbitrary* mesoscopic length D, i.e., beyond the regime of the "small needle expansion".

B1. These exact results have been derived in Sec. III and Appendix B for the free energy of a needle in the half plane with an orientation perpendicular to its boundary i and of a needle embedded along the midline of a strip of infinite length and with the two boundaries being members of the same surface universality class $(i = j)$. These geometries are related to the $W \times L$ strip without a needle (Appendix A 2) via conformal transformations of the Schwarz-Christoffel type [63]. For various combinations (h,i) of the surface universality classes these effective interactions are shown in Figs. 3-5 and display the crossover between the small needle regime and the limiting behavior for which the needle approaches and nearly touches the boundary or becomes much longer than the width of the strip.

B2. Apart from the importance in their own right these universal results allow us to better understand the

limitations of the "small needle approximation". For example, in Fig. 3(a), for $(i[h]) = (-[+])$ this approximation reproduces the exact result for $F_\perp^{(-[+])}$ very well down to a distance of the closer end of the perpendicular needle from the boundary corresponding to half its length ($a_< = D/2 = a_N/2$ so that $\vartheta = D/(2a_N) = 0.5$). For even smaller distances the approximation develops an unphysical maximum, which is the counterpart of the minimum produced by the approximation for ΔF in the case $(-[+]-)$ (see Fig. 15). In contrast, the exact result crosses over to a logarithmic increase which diverges when the needle "touches" the boundary. We recall that the validity of the "small needle approximation" requires that the mesoscopic length D of the needle is small compared with the distance $a_<$ between the closer end of the needle and the boundary, whereas the exact result is valid if only the microscopic lengths are sufficiently small compared with $a_<$. Concerning the free energy $F_\parallel^{(-[+]-)}$ for embedding a $+$ needle extending along the midline of a $(-,-)$ strip, Fig. 4 explicitly demonstrates the ensuing improvement if one expands the corresponding partition function rather than the free energy in terms of the needle length (see the remarks above Eq. (2.16) and in the first and second paragraph of Subsec. V C).

(C) Our results allow us to conclude which of the features studied here are of a more general character and thus can be expected to show up also in spatial dimension $d = 3$ and which ones are specific for $d = 2$.

C1. In dimensions $d > 2$ nonspherical mesoscopic particles such as uniaxial ellipsoids [13, 14] or dumbbells of two touching or interpenetrating spheres of equal size [13] in a half space and interacting with its planar boundary wall have been considered for various universality classes $(i[h])$. Both for particle sizes small [13, 64] and comparable [14] with respect to the distance from the wall, these particles prefer, at *fixed particle center*, orientations perpendicular (parallel) to the boundary of the half space if $i = h$ ($i \neq h$). These are the same preferences as described in paragraph (i) above for our small needles in the half plane. In the mean-field treatment of Ref. [14] it was pointed out that at *fixed closest surface-to-surface distance* of particle and wall the preferred orientations display the opposite trend, i.e., being parallel (perpendicular) to the boundary of the half space if $i = h$ ($i \neq h$). These latter preferences are in agreement with our finding in $d = 2$ that the free energy $F_\parallel^{(i[h])} - F_\perp^{(i[h])}$, required to turn a long needle in the half plane about its closer end from the perpendicular to the parallel orientation, is dominated by the first term, $F_\parallel^{(i[h])} = k_B T \Delta_{i,h} D/a_<$ (note the signs of $\Delta_{i,h}$ given below Eq. (2.9)). The reason is that the

second term, given by Eq. (3.10), depends only logarithmically on the large ratio $D/a_<$ of the needle length D and the distance $a_<$ of the closer end of the needle from the boundary and thus can be neglected relative to the linear increase exhibited by $F_\parallel^{(i[h])}$.

C2. However, there are also effects which are specific to two dimensions, due to the symmetries based on the duality transformation and the much wider class of conformal mappings. For example, the aforementioned equality of the particle insertion free energies as function of v_N for the cases $(O[+]O)$ and $(+[O]+)$ with infinite strip length - based on the duality symmetry [38, 44] of the $d = 2$ Ising model at the bulk critical point - has no correspondence for a particle between parallel walls in $d > 2$. Likewise, the independence of h of the leading small particle contribution ΔF_l to the quasi-torque ΔF in the case $(O[h]O)$ (see Eq. (2.17)) is valid in $d = 2$ but not in $d > 2$. The derivation of this result in $d = 2$ hinges on using a conformal transformation as described in Ref. [40] which is not available for a non-spherical particle in $d > 2$.

C3. There is an interesting difference between "ordinary" needles in $d = 2$ and $d = 3$ which arises from the dependence on their *width* $\mathcal{W}$. Here we have considered needles with a mesoscopic width $\mathcal{W}$ which is much smaller than the needle length D. For both "ordinary" and "normal" needles in $d = 2$ the effects they induce in the embedding critical system (such as the density profiles), and thus their effective interactions with the boundaries leading to force and torque, only depend on their length D but not [65] on their width $\mathcal{W}$. This applies also [66] to a "normal" needle in $d = 3$. However, for an "ordinary" needle in $d = 3$ with fixed length D the strength of these effects decreases [67] upon decreasing the width $\mathcal{W}$. For example, within the small needle expansion the prefactor of the energy density $\mathcal{O} = \epsilon$ is proportional to $D\mathcal{W}^{x_\epsilon - 1} = D\mathcal{W}^{0.42}$ in $d = 3$ while in $d = 2$ it is proportional to $D^{x_\epsilon} = D$ and independent of $\mathcal{W}$ (see Eq. (2.2) and Ref. [23]).

Extending our detailed investigations to non-spherical particles in *three* spatial dimensions and for the whole neighborhood [68] of the critical point is desirable but beyond the scope of the present study. For Monte Carlo simulations in $d = 3$, studies of (square shaped) disks and of "normal" needles with their properties being independent of their width look most promising [65]. Corresponding quantitative analytical predictions remain a challenge. The "small particle expansion" can in principle be extended to, e.g., a circular disk. However, the amplitudes and averages of the corresponding operators can be obtained only approximately. A mean field treatment corresponding to $d = 4$ is given in Ref. [13] but al-

ready one-loop field theoretic calculations, corresponding to the first order contribution in an expansion in terms of $4 - d$, look quite demanding.

Appendix A: STRIP WITHOUT NEEDLE

1. Double periodic boundary conditions

The behavior near bulk criticality of finite Ising strips with periodic boundary conditions in both Cartesian directions has found a long lasting theoretical interest, starting to the best of our knowledge in 1969 with the seminal paper [46] by Ferdinand and Fisher. Therein the aspect ratio dependence of the free energy is given explicitly and was re-derived by other methods in later studies. The quantity $-\Phi_{\rm ST}^{(P)}$ addressed below Eqs. (2.18) and (5.1) is given by the scale free part of $\ln Z_{nm}$ in Eq. (3.37) of Ref. [46]. It is equal to $\ln Z^I$ in Ref. [47] and to $\ln Z_{PP}$ for the Ising model in Ref. [43]. Adopting Cardy's notation (see Eqs. (2.4)-(2.6) and Table 1 in Ref. [43]) the relation for the Casimir (or stress tensor) amplitude Δ_P given below our Eq. (2.18) yields the result

$$\Delta_P(W/L) \equiv \Delta_P(1/\delta) = -\pi/12 - (d/d\delta)\ln\{[\chi_{11}(\delta)]^2 \\ + [\chi_{21}(\delta)]^2 + [\chi_{22}(\delta)]^2\} \quad \text{(A1)}$$

where for the Ising model one has the conformal charge $c = 1/2$ and the parameter $m = 3$ in the functions χ_{pq} introduced by Cardy.

The energy density $\langle \epsilon \rangle_{\rm ST} = f_\epsilon^{(P)}(W/L)/W$ defined below Eqs. (2.3) and (5.1) is of course independent of u and v and turns out to vanish [46, 70] for strips of infinite length L, i.e., $f_\epsilon^{(P)}(0) = 0$. The aspect ratio dependence has been determined in Refs. [46] and [47] and in our notation reads

$$f_\epsilon^{(P)}(W/L) \equiv f_\epsilon^{(P)}(1/\delta) = -\pi E(\delta)/Z(\delta) \quad \text{(A2)}$$

where

$$E(\delta) = [U^{1/24}\Pi_{n=1}^\infty(1 - U^n)]^2 \quad \text{(A3)}$$

with $U = \exp(-2\pi\delta)$ and

$$Z(\delta) = (1/2)\{2E(2\delta)/E(\delta) + [E(\delta)]^2/[E(2\delta)E(\delta/2)] \\ + E(\delta/2)/E(\delta)\}. \quad \text{(A4)}$$

Our quantities $f_\epsilon^{(P)}$, δ, E, and Z correspond to the quantities $-\langle\epsilon\rangle^I$, $-i\tau$, $|\eta^2|$, and Z^I, respectively, in Ref. [47] (see the introductory remarks in Sec. III and Eqs. (3.3), (3.4), and (3.14) therein).

2. Strip with boundaries (i, j)

For our strip (ST) with the aspect ratio $1/\delta = W/L$ and boundaries

$$(i, j) = [(O,O), (+,+), (+,-), (+,O)] \quad \text{(A5)}$$

Cardy's results [43] for the partition functions and our Eqs. (2.8) and (2.9) yield

$$\Delta_{i,j}(1/\delta) = -\pi/48 - (d/d\delta)\ln[\chi_{11}(\delta/2) + \chi_{21}(\delta/2), \\ \chi_{11}(\delta/2), \chi_{21}(\delta/2), \chi_{22}(\delta/2)] \quad \text{(A6)}$$

for the universal stress tensor amplitudes in terms of the functions χ_{pq} introduced in Ref. [43]. For later reference we rewrite Cardy's expressions in the form

$$\Delta_{i,j}(1/\delta) = (\pi/48)\bigg(-1 + 12\kappa(d/d\kappa)\ln\Big\{[\Sigma_{11} + \Sigma_{21}, \\ \Sigma_{11}, \Sigma_{21}, \Sigma_{22}]\Pi_{n=1}^\infty(1 - \kappa^{4n})^{-1}\Big\}\bigg) \quad \text{(A7)}$$

and alternatively as

$$\Delta_{i,j}(1/\delta) = (\pi\delta^{-2}/12)\bigg(1 - 24\sigma(d/d\sigma)\ln\Big\{\Big(1 + \\ + [(\mathcal{S}_{11} + \mathcal{S}_{21})/2, \mathcal{S}_{11}, \mathcal{S}_{21}, \mathcal{S}_{22}]\Big)\prod_{n=1}^\infty(1 - \sigma^{2n})^{-1}\Big\}\bigg) \\ \text{(A8)}$$

which converge rapidly for long strips with large δ (corresponding to extended, closely spaced boundaries) and for short strips with small δ (i.e., short, widely separated boundaries), respectively. In Eqs. (A7) and (A8) one has

$$\kappa = e^{-\pi\delta/4}, \quad \Sigma_{pq} \equiv \Sigma_{pq}(\kappa) = \\ = \sum_{l=-\infty}^\infty \bigg(\kappa^{[(24l+4p-3q)^2-1]/12} - (q \to -q)\bigg)\text{(A9)}$$

and

$$\sigma = e^{-2\pi/\delta}, \quad \mathcal{S}_{pq} \equiv \mathcal{S}_{pq}(\sigma) = \sum_{r=2}^\infty \sigma^{(r^2-1)/24} \times \\ \times \sin\frac{\pi pr}{3}\sin\frac{\pi qr}{4}\Big/\Big(\sin\frac{\pi p}{3}\sin\frac{\pi q}{4}\Big), \quad \text{(A10)}$$

respectively. The three functions $\Sigma_{pq}(\kappa)$ in Eq. (A7) can be written as

$$\Sigma_{pq}(\kappa) = \kappa^{[(4p-3q)^2-1]/12}\Big(1 + \sum_{n=1}^\infty a_n\kappa^{4n}\Big) \quad \text{(A11)}$$

where the coefficients a_n take the integer values $0, \pm 1$ as determined by (A9). For small σ the three functions $S_{pq}(\sigma)$ have the following explicit forms:

$$\begin{aligned} \mathcal{S}_{11} &= 2^{1/2}\sigma^{1/8} + \sigma - \sigma^2 - 2^{1/2}\sigma^{4+1/8} - \sigma^5 + ... \\ \mathcal{S}_{21} &= -2^{1/2}\sigma^{1/8} + \sigma - \sigma^2 + 2^{1/2}\sigma^{4+1/8} - \sigma^5 + ... \\ \mathcal{S}_{22} &= -\sigma - \sigma^2 + \sigma^5 + ... \quad . \end{aligned} \quad \text{(A12)}$$

For closely spaced boundaries with $i \neq j$ the derivative with respect to κ in Eq. (A7) contributes due to the prefactor in Eq. (A11) even in leading order $W/L \ll 1$ so that $\Delta_{i,j}(0)$ depends on (i,j) as given below Eq. (2.9). For widely spaced boundaries (i,j) the derivative with respect to σ in Eq. (A8) does not contribute to the leading behavior and

$$\Delta_{i,j}(1/\delta) \to \pi\delta^{-2}/12 = -\Delta_P(0)/\delta^2, \quad 1/\delta \to \infty,$$
(A13)

is independent of (i,j). In this case of $W/L \gg 1$ the stress tensor averages of the strip ST are dominated by the periodic boundary condition in u direction and determined by $\langle T_{\|\|}\rangle_{\text{ST}} \equiv \langle T_{uu}\rangle_{\text{ST}} \to \Delta_P(0)/L^2$ with $\Delta_P(0)$ given below Eq. (2.18).

The above expressions in Eqs. (A5)-(A12) do not only serve to provide the aspect ratio dependence of the leading contribution ΔF_l in Eq. (2.17) of the free energy required to rotate the small needle in the strip, but also to calculate the effective interactions for certain particles of *arbitrary* size: in the first entry of Ref. [22] for two particles of circular shape as well as in Appendix B 2 below for certain configurations of two needles in the unbounded plane, of one needle in the half plane, and of one needle in a strip.

Now we present the explicit forms of the scaling functions $f_{\mathcal{O}}^{(i,j)}(v_N/W, 0)$ of the density profiles in Eq. (2.7) in a strip of infinite length $L = \infty$. These can be inferred from, e.g., Ref. [49]. In our notation they are given by

$$f_{\phi}^{(O,O)} = 0 \ , \quad f_{\epsilon}^{(O,O)} = C/2$$
$$f_{\phi}^{(+,+)} = (2C)^{1/8} \ , \quad f_{\epsilon}^{(+,+)} = -C/2$$
$$f_{\phi}^{(+,-)} = -(2C)^{1/8}s \ , \quad f_{\epsilon}^{(+,-)} = (C/2)[3 - 4s^2]$$
$$f_{\phi}^{(+,O)} = (C/2)^{1/8}[1-s]^{1/4} \ , \quad f_{\epsilon}^{(+,O)} = (C/2)s$$
(A14)

where

$$C \equiv \pi/\cos(\pi v_N/W), \quad s \equiv \sin(\pi v_N/W). \quad \text{(A15)}$$

One can easily check that near the boundaries the corresponding profiles $\langle \mathcal{O}(\mathbf{r}_N)\rangle$ reduce to the half plane limits $\langle \mathcal{O}(\mathbf{r}_N)\rangle_{\text{half plane}}$ with the amplitudes provided in Eq. (2.5). In particular, in the strip with $i = +$ the three profiles $f_{\phi}^{(+,j)}$ given in Eq. (A14) exhibit the behavior $f_{\phi}^{(+,j)}(v_N/W \to -1/2) \to 2^{1/8}((v_N/W) + (1/2))^{-1/8} = (2W/a_N)^{1/8}$ corresponding to the half plane with boundary $+$.

Appendix B: NEEDLES OF ARBITRARY LENGTH

1. Symmetry preserving cases

Needle and both boundaries belonging to O

Here we establish Eqs. (3.2) and (3.13) for the free energy associated with the insertion of a needle in the case that both the needle and the boundaries are of the symmetry preserving "ordinary" type. We start with Burkhardt's result [69] for the thermal average of the stress tensor induced by n nonoverlapping "ordinary" needles embedded in the x axis of the unbounded (x,y) plane. If the n needles extend from $x_{1<}$ to $x_{1>}$, from $x_{2<}$ to $x_{2>}$, ... , and from $x_{n<}$ to $x_{n>}$, respectively, with arbitrary real numbers $x_{1<} \leq x_{1>} \leq x_{2<} \leq x_{2>} \leq ... \leq x_{n<} \leq x_{n>}$, the stress tensor averages $\langle T_{kl}(x,y)\rangle$ at a point (x,y) follow from the analytic function

$$\langle T(z)\rangle^{([O][O]...[O])} = 2^{-6}\left(\frac{1}{z - x_{1<}} - \frac{1}{z - x_{1>}}\right.$$
$$\left. + \frac{1}{z - x_{2<}} - \frac{1}{z - x_{2>}} + ... + \frac{1}{z - x_{n<}} - \frac{1}{z - x_{n>}}\right)^2$$
(B1)

of the complex variable $z = x + iy$ via [71] the relations $\langle T_{xx}(x,y)\rangle = -\langle T_{yy}(x,y)\rangle = -\text{Re}\langle T(z)\rangle/\pi$ and $\langle T_{xy}(x,y)\rangle = \langle T_{yx}(x,y)\rangle = \text{Im}\langle T(z)\rangle/\pi$ where Re and Im denote real and imaginary parts, respectively. We point out the consistency of Eq. (B1) in the special cases $x_{m<} \to x_{m>}$, in which the needle m disappears, and for $x_{m>} \to x_{m+1<}$, in which two consecutive needles m and $m+1$ merge into a single one. For $n = 1$ this reproduces the expression $\langle T(z)\rangle^{([h])}$ which is independent [40] of h and follows from mapping the half plane onto the entire plane outside a single needle (cp. Eqs. (A8) and (A9) in Ref. [23].

In order to derive Eq. (3.2) we use Eq. (B1) for $n = 2$, put $(x_{1<}, x_{1>}) = (-\infty, 0)$, so that the first needle fills the negative x-axis, and denote $(x_{2<}, x_{2>})$ by $(x_<, x_>)$. The conformal transformation $z = c^2/l$ with $c = a + ib$ maps the (x,y) plane with the two "ordinary" needles onto the half plane $(a > 0, b)$ with the "ordinary" boundary line $a = 0$ and a single embedded "ordinary" needle extending from $(a = \sqrt{lx_<} \equiv a_<, b = 0)$ to $(a = \sqrt{lx_>} \equiv a_>, b = 0)$. This leads to a stress tensor function

$$\langle T(c)\rangle = -A/8 + c^2 A^2/16 \quad \text{(B2)}$$

where

$$A = \frac{1}{c^2 - a_<^2} - \frac{1}{c^2 - a_>^2}. \quad \text{(B3)}$$

In order to obtain this result one uses the transformation formula for the stress tensor which includes the Schwartz derivative [71]. The arbitrary length l, introduced for dimensional reasons, does not appear in the relation between $\langle T(c)\rangle$ and $a_<, a_>$. Shifting the needle away from the boundary line, i.e., increasing the distance $a_N = (a_> + a_<)/2$ of its midpoint from the boundary while keeping its length $a_> - a_<$ and orientation fixed, leads to a change in the free energy $F_\perp$ determined

by [22, 37]

$$\frac{\partial}{\partial a_N}\frac{F_\perp}{k_B T} = -\int_{-\infty}^{\infty} db\,\langle T_{\perp\perp}(a,b)\rangle \qquad (B4)$$

where $\langle T_{\perp\perp}(a,b)\rangle = -\text{Re}\langle T(c)\rangle/\pi$ is the diagonal stress tensor component perpendicular to the boundary line $a = 0$. The integration path must extend between the boundary and the needle, i.e., $0 \le a < a_<$ in Eq. (B4). In this region the integral over b is independent of a and is carried out most easily for $a = 0$. Integrating the result with respect to a_N and denoting the needle length $a_> - a_<$ by D leads to the result in Eq. (3.2) for $F_\perp \equiv F_\perp^{(O[O])}$.

In order to establish Eq. (3.13) one uses the transformation $c/l = \exp(\pi w/W)$, $w = u + iv$, in order to map the half plane $(a > 0, b)$ with its embedded needle onto a needle in strip geometry as described in the context of Eq. (3.13). With the ends of the needle at $u = \pm D/2$, this way one finds the stress tensor function

$$\langle T(w)\rangle = (\pi/W)^2(-1/48 - B/8 + B^2/16) \qquad (B5)$$

where

$$B = \frac{\sinh\theta}{\cosh\theta - \cosh(2\pi w/W)} \qquad (B6)$$

with θ defined in Eq. (3.11). The free energy change $(d/dW)F_\parallel^{(O[O]O)}/(k_B T)$ upon widening the strip follows from the right hand side of Eq. (B4) by replacing (a,b) by (u,v) and identifying $\langle T_{\perp\perp}(u,v)\rangle$ with $\text{Re}\langle T(w)\rangle/\pi$. Here and below Eq. (B4) the real parts of $\langle T(w)\rangle$ and $\langle T(c)\rangle$ enter with a plus and minus sign, respectively, because in the complex w and c planes the directions $\perp$ perpendicular to the boundaries point along the imaginary and the real axis, respectively. Performing the integral and integrating with respect to W leads to the result for $F_\parallel^{(O[O]O)}$ given in Eq. (3.13).

Needle in a strip with periodic boundary condition

Now we consider the geometry corresponding to Eq. (3.16). For the infinitely long strip with periodic boundary condition containing a needle in parallel direction the stress tensor function $\langle T(w)\rangle$ follows from Eq. (B1) with $n = 1$ and the transformation $z/l = \exp(2\pi w/W)$ yielding

$$\langle T(w)\rangle = (\pi/W)^2(-1/12 + B^2/16) \qquad (B7)$$

with B given in Eq. (B6). Proceeding as for the (O, O) strip above, Eq. (B7) leads to the result for $F_\parallel$ given in Eq. (3.16).

Ordinary needle and $+$ boundaries

Finally, we derive Eqs. (3.3) and (3.14) from the expression [69]

$$\langle T(z)\rangle^{([E][O])} = 2^{-6} \times$$
$$\times\left(\frac{1}{z - x_{1<}} - \frac{1}{z - x_{1>}} - \frac{1}{z - x_{2<}} + \frac{1}{z - x_{2>}}\right)^2 \qquad (B8)$$

for the stress tensor function induced by an "extraordinary" needle E extending from $x_{1<}$ to $x_{1>}$ and an "ordinary" needle from $x_{2<}$ to $x_{2>}$. An "extraordinary" needle preserves the $(+ \leftrightarrow -)$ symmetry and can be realized in a lattice model as a line of spins with infinitely strong nearest neighbor ferromagnetic couplings between them so that they all point either in the $+$ or all in the $-$ direction [38, 44]. The partition function $Z^{([E][O])} \equiv Z^{([+][O])} + Z^{([-][O])}$ in the presence of the two needles E and O differs by only a factor of 2 from the two identical partition functions $Z^{([+][O])} = Z^{([-][O])}$ in the presence of two needles $+$ and O or $-$ and O. (This argument holds if the partition functions are finite. This can be achieved by enclosing the whole system in a large box with "ordinary" boundaries.) Thus the corresponding free energies differ by an additive constant $-k_B T \ln 2$ which drops out from the free energy difference upon changing the needle geometry as well as from the stress tensor so that

$$\langle T(z)\rangle^{([E][O])} = \langle T(z)\rangle^{([+][O])} = \langle T(z)\rangle^{([-][O])}. \qquad (B9)$$

Note the different sign sequences in $\langle T(z)\rangle^{([E][O])}$ on the rhs of Eq. (B8) and in $\langle T(z)\rangle^{([O][O])}$ on the rhs of Eq. (B1) with $n = 2$. This implies that for obtaining the $(+[O])$ case Eqs. (B2) and (3.2) have to be modified by replacing $A \to -A$ and $\vartheta \to -\vartheta$, respectively, which leads to Eq. (3.3). Similarly, for the $(+[O]+)$ case Eqs. (B5) and (3.13) have to be modified by replacing $B \to -B$ and $\theta \to -\theta$, respectively, in order to obtain Eq. (3.14).

2. Cases with genuinely broken symmetry

In this subsection we derive the general expressions in Eqs. (3.4) and (3.15) for the Casimir forces which encompass also the cases $(+[+])$, $(-[+])$ and $(+[+]+)$, $(-[+]-)$ which cannot be reduced to cases with symmetry preserving boundaries. We start by considering two needles 1 and 2 on the x axis, similar as in Appendix B 1, but with *arbitrary* universality classes $[i]$ and $[j]$, respectively. The corresponding stress tensor $\langle T(z)\rangle^{([i][j])}$ can be inferred from the difference

$$\langle T(z)\rangle^{([i][j])} - \langle T(z)\rangle^{([O][O])} =$$
$$= \frac{1}{(z - x_{1<})(z - x_{1>})(z - x_{2<})(z - x_{2>})} \times$$
$$\times\frac{(x_{1>} - x_{1<})(x_{2>} - x_{2<})}{(1 - k)^2}\tau_{i,j}(k) \qquad (B10)$$

where

$$\tau_{i,j}(k) = \frac{1}{48}(-1 + 6k - k^2) - \frac{\pi\Delta_{i,j}(1/\delta)}{(2K(k))^2} \qquad (B11)$$

and $\langle T(z)\rangle^{([O][O])}$ is the stress tensor for two "ordinary" needles given by Eq. (B1) with $n = 2$. The quantity $0 \le k \le 1$ is related to cross ratios of the four needle end

points via one of the two following equivalent relations:

$$\frac{(x_{1>} - x_{1<})(x_{2>} - x_{2<})}{(x_{2<} - x_{1>})(x_{2>} - x_{1<})} = \frac{(1-k)^2}{4k} \qquad \text{(B12)}$$

and

$$\frac{(x_{2<} - x_{1<})(x_{2>} - x_{1>})}{(x_{2<} - x_{1>})(x_{2>} - x_{1<})} = \frac{(1+k)^2}{4k}. \qquad \text{(B13)}$$

The amplitude functions $\Delta_{i,j}(1/\delta)$ are given by Eqs. (A6) - (A10) with the argument $1/\delta$ related to k via

$$1/\delta = K(k)/K^*(k) \qquad \text{(B14)}$$

with the complete elliptic integral [52] functions $K(k)$ and $K^*(k) = K(\sqrt{1-k^2})$ (see Eq. (3.8)).

Note that the pole of second order at z equal to a needle end, present with equal residues 2^{-6} in the stress tensor averages in Eqs. (B1) and (B8), is absent in the difference of averages in Eq. (B10). This implies that, e.g., near the needle end at $x_{1<}$ the leading contribution to the corresponding average of the stress tensor elements T_{kl} (see below Eq. (B1)) is independent not only [40] of the length and universality class of needle 1 but also of the presence (i.e., distance, length, and universality class) of another needle 2. Moreover - as shown by Eqs. (B2), (B5), and (B7) above as well as by Eqs. (B17) and (B28) below - this contribution is also independent of the presence of the concomitant boundaries of the half space and the strip.

Equations (B10) - (B14) follow from the Schwarz-Christoffel transformation [63, 72] which conformally maps the $z = x + iy$ plane with the two needles $[i]$ and $[j]$ embedded in the x axis onto the rectangle or strip ST with boundaries (i,j) at $v = \pm W/2$, periodic boundary condition in u direction, and Casimir amplitudes $\Delta_{i,j}$, as introduced in the paragraph containing Eqs. (2.7)-(2.9). The Schwartz derivative in the corresponding transformation law of stress tensors[37, 71] drops out from the stress tensor difference given by Eq. (B10).

The vanishing of $\tau_{i,j}$ in Eq. (B11) for $(i,j) = (O,O)$ provides, together with Eq. (B14), another expression for $\Delta_{O,O}(1/\delta)$ besides (but equivalent to) the ones in Eqs. (A6), (A7), and (A8). For $\Delta_{+,O}(1/\delta)$ the corresponding other expression follows from Eqs. (B10) and (B11) with $(i,j) = (+,O)$ when combined with Eqs. (B1), (B8), and (B9).

The difference of the stress tensors in Eq. (B10) must vanish in the limit of distant needles with no correlation between them because the stress tensor for a single needle in unbounded space is independent of its universality class [40]. For the same reason it must also vanish if two needles of the same universality class $i = j = +$ (or $-$) come close so that they merge, i.e., $x_{1>} = x_{2<}$, and form a single $+$ (or $-$) needle. These expectations are in agreement with the behaviors

$$\lim_{k \to 1} \tau_{i,j}(k) = 0 \qquad \text{(B15)}$$

and

$$\lim_{k \to 0} \tau_{i,j}(k) = [\Delta_{i,i}(0) - \Delta_{i,j}(0)]/\pi \qquad \text{(B16)}$$

of $\tau_{i,j}$ for distant and close needles with $\delta \searrow 0$, $k \nearrow 1$ and $\delta \nearrow \infty$, $k \searrow 0$, respectively. Equation (B15) follows from Eqs. (A13) and (B14).

Proceeding as described above Eq. (B2), the difference of the stress tensors for the needle in the half plane is obtained as

$$\langle T(c) \rangle^{(i[j])} - \langle T(c) \rangle^{(O[O])} = -\frac{4A}{(1-k)^2} \tau_{i,j}(k) \quad \text{(B17)}$$

with $\langle T(c) \rangle^{(O[O])} \equiv \langle T(c) \rangle$ from Eq. (B2) and the function A from Eq. (B3). Via

$$a_</a_> = 2k^{1/2}/(1+k),$$
$$k = (1-\vartheta^{1/2})^2/(1+\vartheta^{1/2})^2 \qquad \text{(B18)}$$

k is related to the needle parameters $a_</a_>$ and $\vartheta = (a_> - a_<)/(a_> + a_<)$ introduced above Eq. (B2) and in Eq. (2.21). Using the relation between k and ϑ in Eq. (B18) together with the suitable functional relations

$$K(k) = (1+\vartheta^{1/2})^2 K^*(\vartheta)/4,$$
$$K^*(k) = (1+\vartheta^{1/2})^2 K(\vartheta) \qquad \text{(B19)}$$

between elliptic integrals (see Eqs. 8.126.1 and 8.126.3 in Ref. [52]) yields together with Eq. (B11) the more convenient expression

$$\frac{4}{(1-k)^2} \tau_{i,j}(k) = \frac{1}{4\vartheta} \tilde{\tau}_{i,j}(\vartheta) \qquad \text{(B20)}$$

for the amplitude in Eq. (B17) where $\tilde{\tau}_{i,j}$ is taken from Eqs. (3.5)-(3.7). Equation (B4) finally yields the expression

$$-\frac{\partial}{\partial a_N} \frac{F_\perp^{(i[j])} - F_\perp^{(O[O])}}{k_B T} = -\frac{1}{4\vartheta} \tilde{\tau}_{i,j}(\vartheta)\left(\frac{1}{a_<} - \frac{1}{a_>}\right) \qquad \text{(B21)}$$

for the difference of the Casimir forces acting on the needle in the cases (i,j) and (O,O) which implies Eq. (3.4) upon renaming the dummy index j as h.

For the special combinations $(+,O)$, $(O,+)$, $(-,O)$, and $(O,-)$ the expression in Eq. (B20) becomes independent of k and ϑ and equals $-1/4$. This follows from comparing Eq. (B10) with the simple expressions in Eqs. (B1) and (B8) and by using Eq. (B9). For combinations (i,j) with both i and j being "normal" universality classes the expression in Eq. (B20) displays a nontrivial dependence on k and ϑ.

In Eq. (3.6) the dependence on ϑ of $\tilde{\tau}_{i,h}$ and $\rho_{i,h}$, with (i,h) being arbitrary, can be readily calculated for a needle nearly touching the boundary ($\bar{\vartheta} = \sqrt{1-\vartheta^2} \searrow 0$, $\delta \nearrow \infty$) as well as for a distant or small needle

$(\vartheta \searrow 0, \delta \searrow 0)$ by combining the first and second expression in Eq. (3.6) with Eqs. (A7) and (A11) and with Eqs. (A8), (A12), and (A13), respectively. In obtaining these limiting behaviors one uses the fact that Eqs. (A9) and (A10) and Eqs. (3.7) and (3.8) imply the simple dependences

$$\kappa = [(\bar{\vartheta}/4)P(\bar{\vartheta}^2)]^2 \,, \quad \sigma = (\vartheta/4)P(\vartheta^2) \qquad \text{(B22)}$$

of κ and σ in Eqs. (A7) and (A8) on $\bar{\vartheta}$ and ϑ, where $P(x^2)$ can be expressed in terms of a power series in x^2 given by

$$P(x^2) = \exp\{-Q(x^2)/R(x^2)\} = 1 + x^2/4 + \mathcal{O}(x^4) \,, \qquad \text{(B23)}$$

with

$$R(x^2) = (2/\pi)K(x) = 1 + x^2/4 + \mathcal{O}(x^4) \qquad \text{(B24)}$$

and (see Ref. [52])

$$Q(x^2) = K(\sqrt{1-x^2}) - R(x^2)\ln(4/x)$$
$$= -2\left\{ \left(\frac{1}{2}\right)^2 \frac{1}{1 \times 2}x^2 + \right.$$
$$\left. + \left(\frac{1 \times 3}{2 \times 4}\right)^2 \left[\frac{1}{1 \times 2} + \frac{1}{3 \times 4}\right]x^4 + ...\right\}. \quad \text{(B25)}$$

We use these relations to show that for small ϑ the exact expressions in Eq. (3.4) for the Casimir forces are consistent with the "small needle expansion". To this end we first note that expanding the expressions in Eq. (3.4) yields

$$-a_N \frac{\partial}{\partial a_N} \frac{F_\perp^{(i[h])}}{k_B T} = -\vartheta \frac{d}{d\vartheta}\ln\{\} + \mathcal{O}(\vartheta^4) \qquad \text{(B26)}$$

with the curly bracket being identical to the curly bracket in the expression for $\Delta_{i,h}$ in Eq. (A8). This follows from inserting Eqs. (3.6) and (A8) into the second expression in Eq. (3.4) and by using Eq. (B24) for $K(\vartheta)$ as well as the relation $\sigma\, d/d\sigma = (1 - \vartheta^2/2 + \mathcal{O}(\vartheta^4))\vartheta\, d/d\vartheta$ due to Eq. (B22). Furthermore, apart from terms of order ϑ^4 the curly bracket in Eq. (B26) is equal to $1 + \zeta_I + \zeta_A$ with the expressions ζ_I and ζ_A from Eq. (2.19) for a small needle in a half plane. For example, in the case $(i[h]) = (-[+])$, with the small needle approximation [41]

$$-a_N \frac{\partial}{\partial a_N}\frac{F_\perp^{(-[+])}}{k_B T} = -\vartheta\frac{d}{d\vartheta}\ln(1 + \zeta_I + \zeta_A)$$
$$= -\vartheta\frac{d}{d\vartheta}\ln[1 - 2^{1/4}\vartheta^{1/8} + \vartheta/4$$
$$- 2^{1/4}(3/32)\vartheta^{2+1/8} + (5/4^3)\vartheta^3] \,, \qquad \text{(B27)}$$

the aforementioned relation between the curly bracket and $1 + \zeta_I + \zeta_A$ follows from the second part of Eq. (A12)

and from Eqs. (B22) and (B23). Accordingly, the difference between the exact expression for the critical Casimir forces in Eq. (3.4) and their small needle approximations is of the order ϑ^4.

Proceeding as in the paragraph containing Eqs. (B5) and (B6), for the geometry of a needle of class j extending along the midline of an (i,i) strip, as discussed in paragraph (ii) in Sec. III, one obtains

$$\langle T(w)\rangle^{(i[j]i)} - \langle T(w)\rangle^{(O[O]O)} = -B \times (\pi/W)^2\, \tilde{\tau}_{i,j}(t)/(4t) \qquad \text{(B28)}$$

with the function B given by Eq. (B6), $\langle T(w)\rangle^{(O[O]O)} \equiv \langle T(w)\rangle$ from Eq. (B5), $\tilde{\tau}_{i,j}$ as in Eq. (3.5), and t related to $\theta \equiv \pi D/W$ as stated in Eq. (3.15). The force in Eq. (3.15) follows from the stress tensor difference in Eq. (B28) upon replacing $[j]$ by $[h]$ and by using a so-called shift equation as in Eq. (B4).

Similar as in the paragraph containing Eq. (B26), the expanded expression

$$-W\frac{\partial}{\partial W}\frac{F_\parallel^{(i[h]i)}}{k_B T} = -2\hat{e}\theta^2 - \theta\frac{d}{d\theta}\ln\{1 + \hat{a}\theta^{1/8} + \hat{b}\theta +$$
$$+ \hat{c}\theta^{2+1/8} + \hat{d}\theta^3\} + \mathcal{O}(\theta^4) \,, \qquad \hat{e} = -(1/3)2^{-7} \,, \text{(B29)}$$

of the exact result in Eq. (3.15) with coefficients $\hat{a} - \hat{e}$ follows from Eqs. (3.6), (A8), (A12), (B22), and (B23) and is related to the "small needle approximation" [41]

$$-W\frac{\partial}{\partial W}\frac{F_\parallel^{(i[h]i)}}{k_B T} = -\theta\frac{d}{d\theta}\ln(1 + \zeta_I - \zeta_A)$$
$$= -\theta\frac{d}{d\theta}\ln(1 + \hat{a}\theta^{1/8} + \hat{b}\theta + \hat{e}\theta^2 + \hat{f}\theta^{2+1/8} + \hat{g}\theta^3) \qquad \text{(B30)}$$

where ζ_I and ζ_A are given by Eqs. (2.13) and (2.14) with needle center $v_N = 0$ at the midline of the (i,i) strip. Note that the term $\hat{e}\theta^2$ with $\hat{e}$ given in Eq. (B29) equals the contribution $(\pi/2)(D/2W)^2\Delta_{i,i}$ with the critical Casimir amplitudes $\Delta_{i,i} = -\pi/48$ for (i,i) strips which enter into ζ_A in Eq. (2.14) and Eq. (B30). Unlike $\hat{e}$, the other coefficients $\hat{a}$, $\hat{b}$, $\hat{c}$, $\hat{d}$, $\hat{f}$, and $\hat{g}$ depend on the boundary and needle universality classes (i,h). The deviation of the exact expression $-W(d/dW)F_\parallel^{(i[h]i)}/(k_B T)$ from its "small needle approximation" is given by the difference of Eq. (B29) and Eq. (B30) and is of the order θ^4 because

$$\hat{a}\hat{e} + \hat{c} - \hat{f} = \hat{b}\hat{e} + \hat{d} - \hat{g} = 0 \,. \qquad \text{(B31)}$$

For example, in the case $(i[h]i) = (-[+]-)$, in which the expression for the argument of the logarithm in Eq. (B30) equals $Z_\parallel$ as given by Eq. (5.4), one has

$$\hat{a} = -2^{1/8}, \ \hat{b} = 1/8, \ \hat{c} = -(5/3)2^{-7+1/8},$$
$$\hat{d} = -(1/3)2^{-9}, \ \hat{f} = -(1/3)2^{-5+1/8}, \ \hat{g} = -2^{-10}, \qquad \text{(B32)}$$

which satisfy Eq. (B31).

For the convenience of the reader we provide the explicit expressions

$$
\begin{aligned}
\left(f^{\perp}_{O[O]}(\vartheta)\right)_{\mathrm{sna}} &= -\ln\{1+(\vartheta/4)[1+(5/16)\vartheta^2]\}, \\
\left(f^{\perp}_{+[+]}(\vartheta)\right)_{\mathrm{sna}} &= -\ln\{1+2^{1/4}\vartheta^{1/8}[1+(3/32)\vartheta^2] \\
&\qquad +(\vartheta/4)[1+(5/16)\vartheta^2]\}, \\
\left(f^{\perp}_{-[+]}(\vartheta)\right)_{\mathrm{sna}} &= -\ln\{1-2^{1/4}\vartheta^{1/8}[1+(3/32)\vartheta^2] \\
&\qquad +(\vartheta/4)[1+(5/16)\vartheta^2]\} \quad \text{(B33)}
\end{aligned}
$$

and

$$
\begin{aligned}
\left(f^{\|}_{O[O]O}(\theta)\right)_{\mathrm{sna}} &= -\ln\Big\{1-(1/3)2^{-7}\theta^2 \\
&\qquad +(\theta/8)[1-2^{-7}\theta^2]\Big\}, \\
\left(f^{\|}_{+[+]+}(\theta)\right)_{\mathrm{sna}} &= -\ln\Big\{1-(1/3)2^{-7}\theta^2 \\
&+(2\theta)^{1/8}[1+(1/3)2^{-5}\theta^2]+(\theta/8)[1-2^{-7}\theta^2]\Big\}, \\
\left(f^{\|}_{-[+]-}(\theta)\right)_{\mathrm{sna}} &= -\ln\Big\{1-(1/3)2^{-7}\theta^2 \\
&-(2\theta)^{1/8}[1+(1/3)2^{-5}\theta^2]+(\theta/8)[1-2^{-7}\theta^2]\Big\}
\end{aligned}
$$
$$
\text{(B34)}
$$

for the [41] "small needle approximations" $(f^{\perp}_{i[h]})_{\mathrm{sna}}$ and $(f^{\|}_{i[h]i})_{\mathrm{sna}}$ of $f^{\perp}_{i[h]} \equiv F^{(i[h])}_{\perp}/(k_B T)$ and $f^{\|}_{i[h]i} \equiv F^{(i[h]i)}_{\|}/(k_B T)$. For the cases $(+[O])$ and $(+[O]+)$ the expressions follow from those for $(O[O])$ and $(O[O]O)$ by the replacements $\vartheta \to -\vartheta$ and $\theta \to -\theta$, respectively.

Appendix C: GLOSSARY

In order to ease the reading of the text, here we compile the symbols and notations used and explain their meanings.

A : Expression given by Eq. (B3) which serves to display the dependence on c of the analytic functions $\langle T(c)\rangle^{(i[h])}$ (see Eqs. (B2) and (B17) as well as the text below Eq. (B9)) and thus to display the position dependence of the stress tensor averages for the geometries of a needle of boundary universality class h in the half plane with orientation perpendicular to the boundary of boundary universality class i.

$\mathcal{A}^{(h)}_{\mathcal{O}}$: Universal amplitudes of the profiles $\langle \mathcal{O}(\mathbf{r})\rangle_{\text{half plane}}$ in the half plane with boundary universality class h where $\mathcal{O} = \phi$ and $\mathcal{O} = \epsilon$ are the normalized operators (see Eq. (2.4)) of the order parameter density and of the deviation of the energy density from its bulk value, respectively (see Eq. (2.5)).

a and b : Half plane coordinates perpendicular and parallel to the boundary $a = 0$ (see above Eqs. (2.5) and (B2)).

a_N : Distance of the needle center from the boundary of the half plane (or from the lower boundary of the strip) (see Fig. 2).

$a_<$ and $a_>$: Distance of the closer and farther needle end from the boundary for a needle in the half plane with perpendicular orientation (see Fig. 2(b) and the text above Eqs. (3.1) and (B2)); $a_> = a_< + D$.

B : Expression given by Eq. (B6) which serves to display the dependence on w of the analytic functions $\langle T(w)\rangle^{(i[h]i)}$ (see Eqs. (B5) and (B28) as well as the text below Eq. (B9)) and thus to display the position dependence of the stress tensor averages for the geometries of a needle of class h embedded in the midline of a strip with (i,i) boundaries.

$c = a + ib$: Complex variable specifying the position vector (a,b) in the half plane (see above Eq. (B2)).

$c_{i,j} \equiv [\Delta F_{nl}/(k_B T)]/(D/W)^2$: Normalized next-to-leading contribution to the quasi-torque acting on a small "ordinary" needle O in an (i,j) strip (see the paragraph following Eqs. (5.2) and (5.3) and the caption of Fig. 10).

D : The number of missing bonds (fixed spins) in the lattice description of the "ordinary" ("normal") needle in Secs. I and IV (see Fig. 1 as well as Figs. 6 and 7) or [27] the length of the needle in the continuum descriptions used in Secs. I, II, III, and Appendix B (see Fig. 2).

E : "Extraordinary" boundary with infinitely strong ferromagnetic nearest neighbor couplings between surface spins (see Ref. [38]).

$F_{\|}$ and $F_{\perp}$: Free energy cost to transfer the needle from the bulk into the strip (or into the half plane) with its orientation parallel and perpendicular to the boundaries, respectively (see Eqs. (2.10)-(2.14) and the text above Eq. (3.11) or below Eq. (3.1)). In particular, $F_{\|} \equiv F^{(i[h]i)}_{\|} = k_B T f^{\|}_{i[h]i}(\theta)$ and $F_{\perp} \equiv F^{(i[h])}_{\perp} = k_B T f^{\perp}_{i[h]}(\vartheta)$ for needles h of arbitrary length embedded in the midline of an (i,i) strip and perpendicular to the boundary i of the half plane, respectively.

$\Delta F \equiv F_{\|} - F_{\perp} \equiv F_1 - F_0$: Free energy required to turn the needle about its center from the perpendicular to the parallel orientation (see Eq. (2.15)).

ΔF_l and ΔF_{nl} : Leading and next-to-leading contributions, respectively, to ΔF for the cases $(i[O]j)$ and $(O[+/-]O)$ of a small needle (see Eqs. (2.16)-(2.18) as well as the corresponding half plane relations in

Eq. (2.20)).

$F_{\mathrm{ST}}^{(i,j)}$: Free energy of the strip ST without needle and with boundaries (i,j) (see Ref. [42]).

$F_{\mathrm{cr}}(\lambda)$: The free energy belonging to the lattice crossover Hamiltonian (see the paragraph containing Eqs. (4.4)-(4.6)).

$f_{i[h]i}^{\parallel}(\theta) \equiv F_{\parallel}^{(i[h]i)}/(k_B T)$: See Eq. (3.12) as well as Figs. 4 and 5.

$f_{i[h]}^{\perp}(\vartheta) \equiv F_{\perp}^{(i[h])}/(k_B T)$: See Fig. 3 and below Eq. (3.1).

f_{b} and f_{s} : Bulk free energy per area and surface free energy per length (see Ref. [42]).

$f_{\mathcal{O}}^{(i,j)}$: Universal scaling functions of the profiles $\langle\mathcal{O}(\mathbf{r})\rangle_{\mathrm{ST}}$ for $\mathcal{O} = \phi,\ \epsilon$ in the needle-free strip ST with boundaries (i,j) (see Eqs. (2.7) and (A14)).

$f_{\epsilon}^{(P)}$: Position-independent universal scaling function of $\langle\epsilon\rangle_{\mathrm{ST}}$ in the needle-free strip ST with double periodic boundary conditions (see below Eq. (2.18) and Appendix A 1).

$g_{i[h]}^{\perp}(\vartheta)$ and $g_{i[h]i}^{\parallel}(\theta)$: Scaling functions for the effective force acting on a needle h perpendicular to the boundary i of the half plane and for the disjoining force induced in an (i,i) strip by a needle h embedded in its midline (see the text below Eq. (3.1) or above Eq. (3.11)).

$\mathcal{H}_{\mathrm{ST}}$: Lattice Hamiltonian for strips without a needle (see Eq. (4.1)).

$\mathcal{H}_{\mathrm{ST}} + \mathcal{H}_{\perp}^{(h)} \equiv \mathcal{H}_0$ and $\mathcal{H}_{\mathrm{ST}} + \mathcal{H}_{\parallel}^{(h)} \equiv \mathcal{H}_1$: Lattice Hamiltonians for strips containing an embedded needle with orientation perpendicular and parallel to the boundaries, respectively (see Eqs. (4.2) and (4.3)).

$\Delta\mathcal{H} \equiv \mathcal{H}_1 - \mathcal{H}_0 \equiv \mathcal{H}_{\parallel}^{(h)} - \mathcal{H}_{\perp}^{(h)}$: Difference of lattice Hamiltonians for parallel and perpendicular orientation of the needle h with a fixed center (see Eqs. (4.4)-(4.7)).

$\mathcal{H}_{\mathrm{cr}}^{(O)}(\lambda)$ and $\mathcal{H}_{\mathrm{cr}}^{(+)}(\lambda)$: Crossover Hamiltonian for the needle of broken bonds and of fixed spins, respectively (see Eqs. (4.10) and (4.19) as well as Figs. 6(c) and 8(c)).

$\tilde{\mathcal{H}}^{(O)}$ and $\tilde{\mathcal{H}}^{(+)}$: Lattice Hamiltonian for a strip containing a cross-shaped hole with the two bars corresponding to the two orientations of the needle of broken bonds and of fixed spins, respectively (see below Eqs. (4.10) and (4.19)).

h : Characterizes the universality class of the needle surface.

(i,j) : Characterizes the surface universality classes of the (lower, upper) boundary of the strip.

$(i[h])$: Needle of class h in the half plane with boundary of class i.

$(i[h]j)$: Needle of class h in the strip with boundaries of classes i and j.

$\mathcal{J} > 0$: Ferromagnetic coupling strength between nearest neighbor Ising spins on the square lattice implying the bulk critical temperature $T_c = [2/\ln(\sqrt{2}+1)](\mathcal{J}/k_B)$ (see Eq. (4.1) and the paragraph above Eq. (4.2)).

$J_{u,v;u',v'}\mathcal{J}$: Coupling between nearest neighbors (u,v) and (u',v') in a strip containing a needle of broken bonds (see Fig. 6(a) and 6(b)). J equals 0 and 1 for broken and unbroken bonds, respectively.

k : Parameter characterizing the configuration of two needles embedded in the x axis of the unbounded (x,y) plane via the cross ratio of their endpoints (see Eqs. (B12) and (B13)).

L : The number of columns in the lattice model for the strips considered in Secs. I and IV (see Fig. 1 and Figs. 6-8) or [27] the length of the strip in the continuum descriptions used in Secs. I, II, III, and Appendix A (see Fig. 2).

l : Arbitrary length in the conformal transformations given in the text above Eqs. (B2), (B5), and (B7) which relate different geometries. It is introduced for dimensional reasons only and, due to dilatation invariance, drops out from equations relating quantities which belong to the same geometry.

$\mathbf{n}$: Unit vector describing the orientation of the needle (see Eq. (2.3)). In the strip, $\mathbf{n} = (n_{\parallel}, n_{\perp})$ (see Eq. (2.6)).

O : The "ordinary" surface universality class. Corresponding boundaries or needles induce disorder in the system of Ising spins, i.e., in their vicinity the probability to find parallel nearest neighbor spins is smaller than in the bulk.

$+$ and $-$: The two "normal" surface universality classes with the tendency to order the Ising spins in the $+$ and $-$ directions, respectively.

$\mathbf{r}_N$: Position vector of the center of the needle (see Eqs. (2.2) and (2.3)). In the strip, $\mathbf{r}_N = (u_N, v_N)$ (see Eq. (2.6)).

S_I and S_A : Operator contribution to the normalized Boltzmann weight of the small needle which is isotropic and anisotropic, respectively, with respect to the orientation of the needle (see Eqs. (2.1)-(2.3)).

ST : Denotes the strip in the absence of the needle.

"sna" ("small needle approximation"): Truncated form of the "small needle expansion" (see the paragraph containing Eqs. (2.16)-(2.18) and the first paragraph of Subsec. V C). For explicit expressions see Eqs. (5.4), (B33), and (B34).

s_0 : Exterior spin fixed to the value $+1$ (see the first paragraph in Sec. IV B 3 as well as Fig. 8(c)).

T_{kl} : Stress-tensor operator (see Eq. (2.3)) with its elements in the strip denoted by $T_{\parallel\parallel}$, $T_{\parallel\perp}$, $T_{\perp\parallel}$, and $T_{\perp\perp}$ (see Eq. (2.8)).

$\langle T(z)\rangle$, $\langle T(c)\rangle$, and $\langle T(w)\rangle$: Analytic functions in the unbounded plane with needles, in the half plane with a needle, and in the strip with a needle, respectively, which determine the corresponding stress tensor averages as explained in Appendix B 1 (see Eqs. (B1), (B2), (B5), (B7)-(B10), (B17), and (B28) as well as Ref. [71]).

$t \equiv \tanh(\theta/2)$: Useful short notation according to Eqs. (3.15) and (B28).

u and v : Strip coordinates [27] parallel and perpendicular, respectively, to the boundaries of the strip. In the continuum description the boundaries of the strip are at $v = \pm W/2$ (see Fig. 2). In the lattice description of a "normal" ("ordinary") needle the coordinates u and v of the lattice vertices have integer (half odd integer) values (see Fig. 1 and Figs. 6-8).

u_N and v_N : Coordinates parallel and perpendicular, respectively, to the strip of the position vector $\mathbf{r}_N = (u_N, v_N)$ of the center of the needle. As explained in Sec. I and Ref. [27], u_N and v_N are lengths in the continuum description used in Sec. II and in Eqs. (A14) and (A15) of Appendix A, while in the lattice description used in Sec. IV they are measured in units of the lattice constant and have integer values for both "ordinary" and "normal" needles.

W : The number of rows in the lattice model for the strip or [27] the width of the strip in the continuum description.

$w = u + iv$: Complex variable specifying the position vector (u, v) in the strip (see above Eq. (B5)).

$x_\phi = 1/8$ and $x_\epsilon = 1$: Scaling dimensions of the order parameter and energy densities, respectively (see below Eq. (2.4)).

$Z_\parallel$ and $Z_\perp$: Partition functions corresponding to $F_\parallel$ and $F_\perp$ (see Eqs. (2.10) and (2.11)).

$Z_{\mathrm{ST}}^{(i,j)}$: Partition function of a $W \times L$ strip ST without needle and with boundaries (i, j) (see Refs. [42] and [44]).

$Z^{([h_1][h_2])}$: Partition function of a large system containing two needles h_1 and h_2 (see below Eq. (B8)).

$z = x + iy$: Complex variable specifying the position vector (x, y) in the unbounded plane (see below Eq. (B1)).

$\Delta_{i,j}(1/\delta)$: Casimir amplitude describing the universal contribution $-L^{-1}\partial\Phi_{\mathrm{ST}}^{(i,j)}(\delta)/\partial W = \Delta_{i,j}(1/\delta)/W^2$ to the disjoining pressure per $k_B T$ of an (i, j) strip without needle (see Eqs. (2.8), (2.9) and Appendix A 2).

$\Delta_{i,j} \equiv \Delta_{i,j}(0)$: Casimir amplitude for an (i, j) strip of infinite length $L = \infty$ and without needle (see below Eq. (2.9)).

$\Delta_P(1/\delta)$: Casimir amplitude for the double periodic strip without needle (see below Eq. (2.18) and Appendix A 1).

$\Delta_P \equiv \Delta_P(0) = -\pi/12$.

$\delta \equiv L/W$: Characterizes the shape of the strip (see Eq. (2.9)). We call $W/L \equiv 1/\delta$ the aspect ratio of the strip.

$\epsilon(\mathbf{r})$: Energy-density operator with its average in the unbounded plane (bulk) at bulk criticality subtracted (see below Eq. (2.3)) and normalized according to Eq. (2.4).

ζ_I and ζ_A : Contributions to $Z_\parallel$ and $Z_\perp$ which arise via the "small needle expansion" from the operator contributions S_I and S_A to the normalized Boltzmann weight of the needle; they are isotropic and anisotropic with respect to the needle orientation, respectively (see Eqs. (2.1)-(2.3), (2.13), and (2.14)).

$\vartheta \equiv D/(2a_N)$: Characterizes the size versus the distance to the boundary for a needle in the half plane with its orientation perpendicular to the boundary line (see Eq. (3.1)).

$\bar\vartheta \equiv \sqrt{1 - \vartheta^2} = \sqrt{a_< a_>}/a_N$: Approaches zero if the closer end of the needle approaches the boundary.

ϑ_0 : Threshold value of ϑ above which the interaction $f_{-[+]}^\perp(\vartheta)$ between a $-$ boundary of the half plane and a $+$ needle perpendicular to it deviates significantly from the corresponding "small needle approximation",

i.e., from the last equation in Eq. (B33) (see the discussion of Fig. 3(a) in the paragraph between Eqs. (3.10) and (3.11)).

$\theta \equiv \pi D/W$: Characterizes the size versus the distance to the boundaries for a needle embedded within the midline of the strip (see Eq. (3.11)).

$\kappa \equiv \exp(-\pi\delta/4)$: Variable used for the aspect ratio dependence of $\Delta_{i,j}$ in the case of a long strip with $L/W \equiv \delta \gg 1$ and close boundaries (see Eqs. (A7) and (A9)).

$\Lambda_i^{(1)}$ and $\Lambda_j^{(1)}$: Strengths of the coupling to the lower and upper additional outside row, respectively, of fixed spins generating strip boundaries i and j of "ordinary" or "normal" character in the lattice model (see Eq. (4.1) and Figs. 1 and 6-8).

λ : Parameter within the lattice model describing the crossover of the needle orientation from perpendicular ($\lambda = 0$) to parallel ($\lambda = 1$) orientation with respect to the boundaries of the strip (see Eq. (4.7) as well as Figs. 6(c) and 8(c)).

$\rho_{i,h}(\vartheta)$: Auxiliary function determining the Casimir force on a needle h in the half plane with boundary i and determining the disjoining force induced in an (i,i) strip of infinite length upon inserting a needle h (see Eqs. (3.4) and (3.15), respectively). Via Eqs. (3.6) and (3.7) the function $\rho_{i,h}(\vartheta)$ is related to the dependence $\Delta_{i,h}(1/\delta)$ on the aspect ratio of the Casimir amplitude of the needle-free strip with boundaries (i,h).

$\sum_{\langle \text{inc.} \rangle}$ and $\sum_{\langle \text{decr.} \rangle}$: Sum of products of those nearest neighbor spins in the crossover Hamiltonian $\mathcal{H}_{\text{cr}}^{(O)}(\lambda)$ the ferromagnetic coupling strength of which increases and decreases, respectively, upon increasing λ (see Eqs. (4.8)-(4.10) and Fig. 6(c)).

$\sum_{\langle \text{one} \rangle}^{(+)}$: Sum of those four spins which are coupled to an external spin (and carry a northeast arrow) for *both* needle orientations shown in Figs. 8(a) and 8(b) (see Eq. (4.16)).

$\sum_{\langle \text{zero} \rangle}$: Sum of products of the center spin of the "normal" (+) needle and of its four nearest neighbor spins (see Eq. (4.13)). These four products are missing in the crossover Hamiltonian $\mathcal{H}_{\text{cr}}^{(+)}$ (see Eq. (4.19)) and the four corresponding couplings are absent in Figs. 8(a), 8(b), and 8(c).

$\widehat{\sum}_{\langle \text{inc.} \rangle}$ and $\widehat{\sum}_{\langle \text{decr.} \rangle}$: Sum of products of those nearest neighbor spins in the crossover Hamiltonian $\mathcal{H}_{\text{cr}}^{(+)}(\lambda)$

the ferromagnetic coupling strength of which increases and decreases, respectively, upon increasing λ (see Eqs. (4.14), (4.15), and (4.19) as well as Fig. 8(c)).

$\sum_{\langle \text{inc.} \rangle}^{(+)}$ and $\sum_{\langle \text{decr.} \rangle}^{(+)}$: Sum of those spins which in the crossover Hamiltonian $\mathcal{H}_{\text{cr}}^{(+)}(\lambda)$ are coupled with increasing and decreasing strength, respectively, to the external spin $s_0 = 1$ (see Eqs. (4.17)-(4.19) and Fig. 8(c)).

$\sigma \equiv \exp(-2\pi/\delta)$: Variable used for the aspect ratio dependence of $\Delta_{i,j}$ in the case of a short strip with $L/W \equiv \delta \ll 1$ and distant boundaries (see Eqs. (A8) and (A10)).

$\tilde{\tau}_{i,h}(\vartheta)$: Auxiliary function with the same character as (and simply related to) $\rho_{i,h}(\vartheta)$ (see Eq. (3.5)).

$\Phi_{\text{ST}}^{(i,j)}(\delta = L/W)$: Universal shape dependent and scale free contribution to the free energy per $k_B T$ of $L \times W$ strips with boundaries (i,j) but without needle (see Eq. (2.8) and Ref. [42]). $\Phi_{\text{ST}}^{(P)}(\delta)$ denotes the corresponding contribution for the double periodic strip.

$\phi(\mathbf{r})$: Order-parameter-density operator, normalized according to Eq. (2.4).

$\chi_{pq}(\delta)$ or $\chi_{pq}(\delta/2)$: Auxiliary functions for the Casimir amplitudes of $W \times L$ strips without a needle and with double periodic boundary conditions or with (i,j) boundaries (see Eqs. (A1) or (A6) as well as Ref. [43]).

$\langle ... \rangle$: Thermal average which may be specified by means of subscripts and superscripts such as

$\langle ... \rangle_{\text{bulk}}$: for the unbounded plane without embedded particles (see Eq. (2.4)).

$\langle ... \rangle_{\text{half plane}}$: for the half plane without embedded particles (see above Eq. (2.5)).

$\langle ... \rangle_{\text{ST}}$ and $\langle ... \rangle_{\text{ST}}^{(i,j)}$: for a strip without embedded particles and with boundaries (i,j) (see Eqs. (2.7) and (2.8)).

$\langle ... \rangle^{(i[h])}$: for the half space with boundary i and an embedded needle h (see Eq. (B17)).

$\langle ... \rangle^{(i[h]j)}$: for the strip with boundaries (i,j) and an embedded needle h (see Eq. (B28)).

$\langle ... \rangle^{([h_1][h_2]..[h_n])}$: for the unbounded plane with n embedded needles h_1, h_2, .., h_n (see Eqs. (B1) and (B8)-(B10)).

$\langle ... \rangle_{\text{cr}}$: Thermal average based on the lattice crossover Hamiltonian (see Eqs. (4.5) and (4.6)).

[1] M.E. Fisher and P.G. de Gennes, C. R. Acad. Sci. Paris, **287**, B-207 (1978).

[2] M. Krech, *The Casimir Effect in Critical Systems* (World Scientific, Singapore, 1994).

[3] I. Brankov, D.M. Danchev, and N.S. Tonchev, *Theory of Critical Phenomena in Finite-Size Systems: Scaling and Quantum Effects* (World Scientific, Singapore, 2000).

[4] A. Gambassi, J. Phys.: Conf. Ser. **161**, 012037 (2009).

[5] R. Garcia and M.H.W. Chan, Phys. Rev. Lett. **83**, 1187 (1999).

[6] A. Ganshin, S. Scheidemantel, R. Garcia, and M.H.W. Chan, Phys. Rev. Lett. **97**, 075301 (2006).

[7] R. Garcia and M.H.W. Chan, Phys. Rev. Lett. **88**, 086101 (2002).

[8] M. Fukuto, Y.F. Yano, and P.S. Pershan, Phys. Rev. Lett. **94**, 135702 (2005).

[9] C. Hertlein, L. Helden, A. Gambassi, S. Dietrich, and C. Bechinger, Nature **451**, 172 (2008).

[10] A. Gambassi, A. Maciolek, C. Hertlein, U. Nellen, L. Helden, C. Bechinger, and S. Dietrich, Phys. Rev. E **80**, 061143 (2009).

[11] M. Kardar and R. Golestanian, Rev. Mod. Phys. **71**, 1233 (1999).

[12] M. Bordag, U. Mohideen, and V. M. Mostepanenko, Phys. Rep. **353**, 1205 (2001).

[13] E. Eisenriegler, J. Chem. Phys. **121**, 3299 (2004).

[14] S. Kondrat, L. Harnau, and S. Dietrich, J. Chem. Phys. **131**, 204902 (2009).

[15] U. Nellen, L. Helden, and C. Bechinger, EPL **88**, 26001 (2009).

[16] (a) K. Binder, in *Phase Transitions and Critical Phenomena*, edited by C. Domb and J.L. Lebowitz (Academic, London, 1983), Vol. **8**, p. 1; (b) H.W. Diehl, in *Phase Transitions and Critical Phenomena*, edited by C. Domb and J.L. Lebowitz (Academic, London, 1986), Vol. **10**, p. 76; (c) H.W. Diehl, Int. J. Mod. Phys. B **11**, 3503 (1997).

[17] O. Vasilyev, A. Gambassi, A. Maciolek, and S. Dietrich, EPL **80**, 60009 (2007).

[18] O. Vasilyev, A. Gambassi, A. Maciolek, and S. Dietrich, Phys. Rev. E **79**, 041142 (2009).

[19] M. Hasenbusch, Phys. Rev. B **81**, 165412 (2010).

[20] R. Evans and J. Stecki, Phys. Rev. B **49**, 8842 (1994).

[21] The neighborhood of the actual second order phase transition in an Ising film system (which, e.g., for $(i, j) = (O, O)$ boundaries appears at a temperature below the bulk transition temperature and at zero bulk field) is characterized by a correlation length $\xi_\parallel$ parallel to the film which is much larger than its width and is governed by long-ranged fluctuations of $d - 1$ dimensional character. The usual expansion in terms of $\varepsilon = 4 - d$ with the mean-field theory as the starting point $(d = 4)$ cannot be expected to work in this region of the spatial dimensional crossover $d \to d - 1$. This has been substantiated for the related crossover phenomena $d \to 1$ and $d \to 0$ in systems with the shape of a tube and a cube, respectively (see the corresponding modified ε-expansions in E. Brezin and J. Zinn-Justin, Nucl. Phys. B **257**, 867 (1985)).

[22] T. W. Burkhardt and E. Eisenriegler, Phys. Rev. Lett. **74**, 3189 (1995); **78**, 2867 (1997); E. Eisenriegler and U. Rietschel, Phys. Rev. B**51**, 13717 (1995).

[23] E. Eisenriegler, J. Chem. Phys. **124**, 144912 (2006).

[24] In order to avoid confusion we stress that the "small" mesoscopic particle has to be sufficiently *large* on the microscopic scale for displaying universal scaling properties. This is the analogue of the "small" distance between the two operators in the operator product expansion to be still sufficiently large.

[25] K.G Wilson and J.B Kogut, Phys. Rep. C **12**, 75 (1974); A. Z. Patashinskii and V. L. Pokrovskii, *Fluctuation Theory of Phase Transitions* (International Series in Natural Philosophy, Vol. **98**, Pergamon, New York, 1979); A. A. Belavin, A. M. Polyakov, and A. B. Zamolodchikov, Nuclear Phys. B **241**, 333 (1984).

[26] The "operators" in the present systems of classical statistical mechanics are classical objects fluctuating with the basic statistical variables (which in the Ising lattice model are the Ising spins). In the operator expansions one uses local operators in coarse grained models (such as the densities of the order parameter and of the energy), see Refs. [13], [23], and [35] as well as the entries in Refs. [22] and [25].

[27] The symbols D, W, L, u, u_N, v, v_N are used with an obvious double meaning. While they are introduced as *numbers* in the lattice model (see the Introduction and Sec. IV) we consider them in the mesoscopic continuum descriptions of Secs. II and III as *lengths* which follow from the corresponding numbers upon multiplication with the lattice constant.

[28] T. Emig, N. Graham, R.L. Jaffe, and M. Kardar, Phys. Rev. A **79**, 054901 (2009).

[29] H. Gies and K. Klingmueller, Phys. Rev. Lett. **97**, 220405 (2006); A. Weber and H. Gies, Phys. Rev. D **80**, 065033 (2009).

[30] R. Roth, R. van Roij, D. Andrienko, K.R. Mecke, and S. Dietrich, Phys. Rev. Lett. **89**, 088301 (2002).

[31] L. Helden, R. Roth, G.H. Koenderink, P. Leiderer, and C. Bechinger, Phys. Rev. Lett. **90**, 048301 (2003).

[32] M. F. Maghrebi, Y. Kantor, and M. Kardar, EPL **96**, 66002 (2011); Phys. Rev. E **86**, 061801 (2012).

[33] B.B. Machta, S.L. Veatch, and J.P. Sethna, Phys. Rev. Lett. **109**, 138101 (2012). While the Monte Carlo results in Figs. 1 and 3 of this paper are new, the corresponding conformal field theory (CFT) results for circular inclusions in the $d = 2$ Ising model at criticality have already been obtained earlier in the paper cited first in the present Ref. [22] (see Fig. 1 therein) by using Cardy's exact partition functions of the finite critical Ising model on a cylinder (see Ref. [43] below) and a conformal mapping onto the geometry with two circles.

[34] Our study is exclusively about properties for which the bulk of the $d = 2$ Ising model is at the critical point. Thus for all expressions shown we correspondingly assume that the temperature is at bulk T_c and that there is no bulk field coupled to the order parameter.

[35] The density operators $\phi(\mathbf{r} = (u, v))$ and $e(\mathbf{r} = (u, v))$ introduced below Eq. (2.3) are the coarse-grained (and normalized) counterparts of the fluctuating values of the spin $s_{u,v}$ and of the nearest neighbor sum $-\mathcal{J} s_{u,v} \sum_{u',v'}' s_{u',v'}$ of the energy contributions, respectively, for the Ising lattice model introduced in Sec. IV.

[36] With the normalization used in Eq. (2.4) the inverse length dimensions of ϕ and ϵ are equal to their scaling dimensions and the half plane amplitudes in Eq. (2.5) are universal.

[37] J.L. Cardy, in *Phase Transitions and Critical Phenomena*, edited by C. Domb and J.L. Lebowitz (Academic, New York, 1986), Vol. 11, p. 55; J.L. Cardy, Nucl. Phys. B **240**, 514 (1984).

[38] Under the duality transformation the bulk of the Ising model remains at the critical point, the energy density operator ϵ turns into $-\epsilon$, and an O boundary of the half plane or strip with a free surface becomes an "extraordinary" (E) boundary [16] with infinitely strong edge couplings (see T. W. Burkhardt, J. Phys. A **18**, L307 (1985)). Likewise, a needle of D missing bonds (as in Figs. 1(a) and 1(b)) becomes a line of $D+1$ spins with infinite couplings between nearest neighbors which can be called an "extraordinary" needle if its length is mesoscopic. For each of these "extraordinary" objects the infinitely strongly coupled spins are in the same type of state (all $+$ or all $-$). Since ϵ is invariant against a simultaneous change of sign of all spins, $\langle\epsilon\rangle_O = -\langle\epsilon\rangle_E = -\langle\epsilon\rangle_+ = -\langle\epsilon\rangle_-$ for energy density profiles in the half plane or around a single needle embedded in the bulk.

[39] For the Ising model in spatial dimensions d larger than 2 the universal half-space amplitudes $\mathcal{A}_\epsilon^{(+)} \equiv \mathcal{A}_\epsilon^{(-)}$ and $\mathcal{A}_\epsilon^{(O)}$ have the same signs as their half-plane counterparts in Eq. (2.5), but their absolute values are not equal any more. Using well-known field theoretic techniques (see, e.g., H.W. Diehl and M. Smock, Phys. Rev. B **47**, 5841 (1993) and B **48**, 6740 (1993) as well as E. Eisenriegler, M. Krech, and S. Dietrich, Phys. Rev. B **53**, 14377 (1996), and references therein) explicit expressions for all amplitudes $\mathcal{A}_\mathcal{O}^{(h)}$, including the energy-density amplitude for a surface belonging to the multicritical "special" surface universality class [16], can be obtained within the $\varepsilon \equiv 4 - d$ expansion about $d = 4$. These results are presented in Ref. [13] and in the first two entries of Ref. [22].

[40] This property is special for two-dimensional conformal models in which the space outside a (simply connected) particle and its surface, embedded in the unbounded plane, can be conformally mapped onto the half plane $a > 0$ and its straight line boundary $a = 0$, respectively. Since the thermal average of the stress tensor in the half plane vanishes for all surface universality classes h, its average outside the particle is solely determined by the Schwartz derivative of the mapping [37] and thus depends only on the shape of the particle and not on its surface class h. This should be compared with the density profiles $\langle\mathcal{O}\rangle_{\text{half plane}} = \mathcal{A}_\mathcal{O}^{(h)} a^{-x_\mathcal{O}}$ in the half plane (see Eq. (2.5)) and the ones outside the particle, which both do depend on h.

[41] For small needles we shall neglect the contributions of fourth or higher order in D which are indicated by the ellipses in Eqs. (2.2), (2.3), (2.13), (2.14), and (2.19). We frequently call this truncated expansion the "small needle *approximation*".

[42] For the strip ST with boundaries (i,j), free energy $F_{\text{ST}} \equiv F_{\text{ST}}^{(i,j)} = -k_B T \ln Z_{\text{ST}}^{(i,j)}$, and partition function $Z_{\text{ST}}^{(i,j)}$ the universal contribution $\Phi_{\text{ST}}^{(i,j)}(L/W)$ introduced above Eq. (2.8) is the limit of $[F_{\text{ST}}^{(i,j)} - WLf_\text{b} - L(f_\text{s}^{(i)} +$

$f_\text{s}^{(j)})]/k_B T$ as L and W tend to infinity with L/W fixed. Here f_b is the bulk free energy per area while $f_\text{s}^{(i)}$ and $f_\text{s}^{(j)}$ are the surface free energies per length corresponding to the surface classes i and j, respectively.

[43] J. L. Cardy, Nucl. Phys. B **275** [FS17], 200 (1986).

[44] While duality implies $\Delta_{O,O} = \Delta_{E,E}$ for *all* values of $\delta = L/W$, the identity $\Delta_{E,E} = \Delta_{+,+}$ and its consequence $\Delta_{O,O} = \Delta_{+,+}$ only hold for long strips with $\delta \gg 1$ for which one can neglect $Z_{\text{ST}}^{(+,-)}$ in the actual expression $Z_{\text{ST}}^{(E,E)} \equiv 2[Z_{\text{ST}}^{(+,+)} + Z_{\text{ST}}^{(+,-)}]$ for the partition function of a strip with two "extraordinary" boundaries. This is expected intuitively and follows formally from $Z_{\text{ST}}^{(+,-)}/Z_{\text{ST}}^{(+,+)} \cong \exp[-\Phi_{\text{ST}}^{(+,-)}]/\exp[-\Phi_{\text{ST}}^{(+,+)}] = \chi_{21}/\chi_{11} \to \exp[-(\pi/2)L/W]$. Here, in the first step, we have used Ref. [42] and the equality $f_\text{s}^{(+)} = f_\text{s}^{(-)}$ and, in the second step, Cardy's results [43] $\exp[-\Phi_{\text{ST}}^{(+,+)}] = \chi_{11} \exp[\pi\delta/48]$ and $\exp[-\Phi_{\text{ST}}^{(+,-)}] = \chi_{21} \exp[\pi\delta/48]$ with $\chi_{pq} \equiv \chi_{pq}(\delta/2)$ as introduced in Ref. [43] for Ising strips with boundaries. (Via Eq. (2.9) these results are, of course, equivalent to our corresponding Eqs. (A6).) For *arbitrary* δ, the above expression for $Z_{\text{ST}}^{(E,E)}$ and Ref. [42] for $(i,j) = (+,+)$ and $(+,-)$ tell that $Z_{\text{ST}}^{(E,E)} \times \exp(WLf_b/(k_B T))$ equals the product of $\exp[-\Phi_{\text{ST}}^{(+,+)}] + \exp[-\Phi_{\text{ST}}^{(+,-)}]$ and a factor which depends on L but not on W. Thus by using the above relations for Φ_{ST} and the relation $\Delta_{E,E} = (W^2/L)\partial_W[\ln Z_{\text{ST}}^{(E,E)} + WLf_b/(k_B T)]$, which follows from Eq. (2.8) and Ref. [42] with $(i,j) = (E,E)$, one confirms that the duality relation $\Delta_{E,E} = \Delta_{O,O}$ is in accordance with Cardy's results in the form of our Eq. (A6).

[45] Unlike $Z_\parallel$, $Z_\perp$ an expansion of $F_\parallel$, $F_\perp$ would involve arbitrary integer powers of $(D/W)^{1/8}$ for a "normal" needle in a strip with at least one "normal" boundary.

[46] A. E. Ferdinand and M. E. Fisher, Phys. Rev. **185**, 832 (1969).

[47] P. di Francesco, H. Saleur, and J. B. Zuber, Nucl. Phys. B **290** [FS20], 527 (1987).

[48] There are two consequences of duality for the energy density scaling functions. The property, that $f_\epsilon^{(+,O)}$ is an odd function of v_N/W, is not only valid for infinite strips $W/L = 0$ (see Eq. (A14)) but even for *arbitrary* values of W/L. However, the identity $f_\epsilon^{(O,O)} = -f_\epsilon^{(+,+)}$ only holds for infinite strips (compare the corresponding arguments for $\Delta_{O,O} = \Delta_{+,+}$ in the present Ref. [44]).

[49] T. W. Burkhardt and T. Xue, Nucl. Phys. B **345**, 653 (1991).

[50] For the needle perpendicular to the boundary of the half plane the dimensionless and universal scaling function $f_{i[h]}^\perp(\vartheta) = F_\perp^{(i[h])}/(k_B T)$ of the free energy is related to the scaling function $g_{i[h]}^\perp(\vartheta) = -a_N(\partial/\partial a_N)F_\perp^{(i[h])}/(k_B T)$ of the force by $f_{i[h]}^\perp(\vartheta) = \int_0^\vartheta d\hat\vartheta g_{i[h]}^\perp(\hat\vartheta)/\hat\vartheta$ because $f_{i[h]}^\perp(\vartheta = 0) = 0$. The corresponding relations for the needle with parallel orientation and at the center line of a symmetric strip follow upon the replacements $F_\perp^{(i[h])} \to F_\parallel^{(i[h]i)}$, $a_N \to W$, $(\vartheta, \hat\vartheta) \to (\theta, \hat\theta)$, and $f_{i[h]}^\perp \to f_{i[h]i}^\parallel$, $g_{i[h]}^\perp \to g_{i[h]i}^\parallel$, where $\theta = \pi D/W$.

[51] Arguing along the lines of Ref. [38] leads to $F_\perp^{(O[+])} = F_\perp^{(+[O])}$.

[52] I. S. Gradsteyn and I. M. Ryshik, *Table of Integrals, Se-*

ries, and Products (Academic, New York, 1965). In this reference the function K^* appearing in Eqs. (3.7), (3.8), (B14), and (B19) is denoted as K'.

[53] The geometry underlying Eq. (3.9) of an infinitely long needle perpendicular to a boundary line is reminiscent of an (idealized) AFM geometry of a cone near a wall (mimicking the surface of a colloidal particle), albeit in two spatial dimensions and for a vanishing opening angle of the cone. It would be interesting to use AFM in order to investigate critical Casimir forces for such a system immersed in a critical binary liquid mixture. The somewhat related critical behavior of the cone-plate interaction induced by a long flexible polymer chain attached to the cone tip has been discussed in Ref. [32]. Still another example for two interacting scale-free objects is provided in Ref. [29] analyzing the quantum-electrodynamical Casimir effect between a plane and a semi-infinite plate. In all these cases only a single length appears and the force between such objects is related, via simple dimensional considerations, to a negative integer power of this length times a universal constant, like in the original geometry of two infinitely extended parallel plates.

[54] The factor π in the definition in Eq. (3.11) simplifies later formulae.

[55] C. H. Bennett, J. Comp. Phys. **22**, 245 (1976).

[56] D. P. Landau and K. Binder, *A Guide to Monte Carlo Simulations in Statistical Physics* (Cambridge University Press, London, 2005), p. 155.

[57] U. Wolff, Phys. Rev. Lett. **62**, 361 (1989).

[58] N. Metropolis and S. Ulam, J. Amer. Stat. Assoc. **44**, 335 (1949).

[59] For any $W \times L$ strip, the leading anisotropic contribution of the average of $\mathcal{O}(\mathbf{r} - \mathbf{s}/2)\mathcal{O}(\mathbf{r} + \mathbf{s}/2)$ with $\mathcal{O} = \phi$ or ϵ (normalized in accordance with Eq. (2.4)) is given by $\langle \mathcal{O}(\mathbf{r} - \mathbf{s}/2)\mathcal{O}(\mathbf{r} + \mathbf{s}/2)\rangle_{\text{ST}}^{(\text{aniso})} = 4\pi x_\mathcal{O}\Delta s^{-2x_\mathcal{O}}(s_u^2 - s_v^2)/W^2$. This result is independent of $\mathbf{r}$ and holds if $|\mathbf{s} = (s_u, s_v)| \equiv s$ is of mesoscopic size but much smaller than W, L, and the distance of $\mathbf{r}$ from the boundaries. In this expression one has $\Delta \equiv \Delta_{i,j}(W/L)$ and $\Delta \equiv \Delta_P(W/L)$ for strips with boundaries (i, j) and double periodic boundary conditions, respectively (see J. L. Cardy, Nucl. Phys. B **290**, 355 (1987) and Ref. [13]). The reason for this position-independent anisotropy of both the two-point average of close operators ($\propto s_u^2 - s_v^2$, see above) and of the free energy $F(\mathbf{r}_N, \mathbf{n})$ of a small particle (see Eqs. (2.3), (2.14), and (2.17)) is the appearance of the stress tensor in the form $\sum_{kl} s_k s_l T_{kl}$ and $\sum_{kl} n_k n_l T_{kl}$, respectively, in the operator expansion of these small objects in the strip. A particularly direct connection between these two types of anisotropies can be established for an anisotropic quasi-particle consisting of two weak point defects a small mesoscopic distance s apart, represented by the perturbation $\delta\mathcal{H} \propto \mathcal{O}(\mathbf{r}-\mathbf{s}/2)+\mathcal{O}(\mathbf{r}+\mathbf{s}/2)$ with $\mathcal{O} = \phi$ or ϵ, and embedded in a double periodic strip. In this case the anisotropic part of the embedding free energy is, apart from a minus sign, proportional to the aforementioned anisotropy $\langle\mathcal{O}(\mathbf{r} - \mathbf{s}/2)\mathcal{O}(\mathbf{r} + \mathbf{s}/2)\rangle_{\text{ST}}^{(\text{aniso})}$ of the two-point average in the strip ST. The sign of Δ_P implies that, like the small needles, this quasi-particle also prefers to align perpendicular to the longer axis of the double periodic strip.

[60] The error bars in Fig. 9 and in Figs. 11-14 depict the standard deviations of numerical simulation data, calculated via averaging over ten series of Monte Carlo steps.

[61] The effect (ii) described in the Summary prevails for cases in which ΔF can be expanded in terms of D and is dominated by its leading order $\propto D^2$. This applies to needle positions near the strip center for the cases $(i[h]j)$ considered in Subsec. V B. However, for the cases considered in Subsec. V C in which the needle is subject to the order parameter profile induced by the boundaries (i, j) there appear terms $\propto (D/W)^{1/8}$ inside the logarithm determining ΔF which cannot be made sufficiently small in simulations with mesoscopic D (in order not to exceed a tractable lattice size $W \times L$) and prevent a useful expansion (see the remarks above Eq. (2.16)). Actually, for the case $(-[+]-)$ the naive application of (ii) would predict the wrong orientation of the needle near the strip center (compare the discussion in the paragraph containing Eq. (5.4)).

[62] For the case $(+[+]-)$ the simulation data and the analytic prediction indicate that ΔF becomes *positive*, in agreement with the observation (i) in the Summary, for values v_N/W which are closer to the $+$ boundary (i.e., which are more negative) than the ones shown in Fig. 15.

[63] See, e.g., V. I. Smirnov, *A Course of Higher Mathematics* (Pergamon, Oxford 1964), Vol. 3.

[64] Unlike in $d = 2$, in *three* spatial dimensions ($d = 3$) the scaling dimension $2+x_\phi$ of $\partial_{r_{Nk}}\partial_{r_{Nl}}\phi$ is *smaller* than the scaling dimension d of the stress tensor. Thus for small "normal" particles with uniaxial shape-symmetry (such as a disk of diameter D or a needle of length D) and located between infinitely extended parallel plates - a distance W apart and with broken symmetry -, the leading orientation dependent contribution within the small particle expansion is proportional to D^{2+x_ϕ} times the second derivative of the order parameter profile in the system without the particle. Moreover with $x_\phi(d = 3) \approx 1/2$ (about four times larger than in $d = 2$) it might be possible within a simulation to keep $(D/W)^{x_\phi}$ and $(D/a_N)^{x_\phi}$ significantly smaller than 1 and to single out the leading quasi-torque ΔF_l proportional to D^{2+x_ϕ}.

[65] Needles in $d = 2$ and disks in $d = 3$ are "impenetrable" boundaries of finite extent D in the sense that spins close but on different sides, separated by the width $\mathcal{W}$ of the boundary with $\mathcal{W} \ll D$, are coupled only via correlations around the ends of the boundary. (This also applies to the needles in the present lattice model with nearest neighbor couplings and where $\mathcal{W}$ is of the order of the lattice constant.) Thus the density profiles they induce at mesoscopic distances much larger than $\mathcal{W}$ are independent of $\mathcal{W}$ and depend only on D. For needles in $d = 3$, however, spins can communicate round about the needle axis. For the "normal" needle the issue arises to which extent its properties, which are independent of their width for small *mesoscopic* widths (see Ref. [66]), can be transferred to the case of a *microscopic* width of a needle represented by spins fixed in a single line of the lattice only.

[66] In $d = 3$ the insertion free energy of a thin "normal" needle is independent of its width $\mathcal{W}$. This independence follows from the corresponding property of a thin cylinder or needle of infinite length discussed in A. Hanke and S. Dietrich, Phys. Rev. E **59**, 5081 (1999) and in A. Hanke, Phys. Rev. Lett. **84**, 2180 (2000).

[67] E. Eisenriegler, J. Chem. Phys. **125**, 204903 (2006).

[68] Moving away from the critical point leads to an even richer diversity in the behavior of the orientation-dependent interactions of non-spherical particles, because the finite correlation length ξ enters as another mesoscopic length besides the lengths L, W, v_N, and D (see the mean-field analysis in Ref. [14]). In the "small particle expansion" additional terms associated with isotropic and anisotropic operators appear which are accompanied by powers of the particle size higher than the leading ones. In the context of the Gaussian model an example is provided by the operator O_{III} in Eq. (2.12) in E. Eisenriegler, A. Bringer, and R. Maassen, J. Chem. Phys. **118**, 8093 (2003).

[69] Equations (B1) and (B8) are unpublished expressions derived by T. W. Burkhardt using the approach presented in T. W. Burkhardt and J.-Choi, Nucl. Phys. B **376**, 447 (1992).

[70] The vanishing of $f_\epsilon^{(P)}$ in the *infinite* strip with periodic boundary condition follows from its vanishing in the unbounded plane, the conformal mapping between these two geometries, and from ϵ transforming as a so-called "primary" operator.

[71] The relations given below Eq. (B1) between $\langle T_{kl}(x,y) \rangle$ and $\langle T(z) \rangle$ are based on the normalization of T_{kl} as specified by Eq. (2.8) and consistent with Eq. (B4). Here $T(z)$ is the usual [37] complex stress tensor which within thermal averages is an analytic function of z and its normalization is specified by its transformation law. For two geometries G and $\tilde{G}$ related by the conformal mapping $z = z(\tilde{z})$, the corresponding analytic functions $\langle T(z) \rangle_G$ and $\langle T(\tilde{z}) \rangle_{\tilde{G}}$ are related by $\langle T(\tilde{z}) \rangle_{\tilde{G}} = (dz/d\tilde{z})^2 \langle T(z) \rangle_G + S/24$ with the Schwartz derivative $S = (z'''/z') - (3/2)(z''/z')^2$ where the primes denote derivatives with respect to $\tilde{z}$. For example, for the mapping $z = z(c) = c^2/l$ considered above Eq. (B2) this relation allows one to obtain $\langle T(c) \rangle_{\tilde{G}} \equiv \langle T(c) \rangle$ in Eq. (B2) from $\langle T(z) \rangle_G \equiv \langle T(z) \rangle^{([O][O])}$ according to Eq. (B1).

[72] For the simple needle configuration $x_{1<} = -1/k$, $x_{1>} = -1$, $x_{2<} = 1$, $x_{2>} = 1/k$ with $0 \leq k \leq 1$ the mapping is provided by $u + iv = i(W/2)[\int_0^z dt/\sqrt{(1-t^2)(1-k^2t^2)}]/K(k)$. This maps the upper and lower halves of the z plane with $y > 0$ and $y < 0$ onto the left and right halves of the rectangle or strip ST with $u < 0$ and $u > 0$, respectively. Crossing the x axis outside of the interval where the needles are, i.e., at $|x| > 1/k$ corresponds to jumping within the rectangle from $(u = -L/2, v)$ to $(u = L/2, v)$ which amounts to the periodic boundary condition in u direction. The more general needle configuration corresponding to Eq. (B10) is related to the simple one by a special conformal transformation which preserves the real axis.